

# The circular internal hydraulic jump

S. A. THORPE<sup>1</sup>† AND I. KAVČIČ<sup>2</sup>

<sup>1</sup>School of Ocean Sciences, Marine Science Laboratories,  
Bangor University, Menai Bridge, Anglesey LL59 5EY, UK

<sup>2</sup>Department of Geophysics, Faculty of Science, University of Zagreb,  
Horvatovac bb, 10000 Zagreb, Croatia

(Received 30 November 2007 and in revised form 13 May 2008)

Circular hydraulic jumps are familiar in single layers. Here we report the discovery of similar jumps in two-layer flows. A thin jet of fluid impinging vertically onto a rigid horizontal plane surface submerged in a deep layer of less-dense miscible fluid spreads radially, and a near-circular internal jump forms within a few centimetres from the point of impact with the plane surface. A jump is similarly formed as a jet of relatively less-dense fluid rises to the surface of a deep layer of fluid, but it appears less stable or permanent in form. Several experiments are made to examine the case of a downward jet onto a horizontal plate, the base of a square or circular container. The inlet Reynolds numbers,  $Re$ , of the jet range from 112 to 1790. Initially jumps have an undular, laminar form with typically 2–4 stationary waves on the interface between the dense and less-dense layers but, as the depth of the dense layer beyond the jump increases, the transitions become more abrupt and turbulent, resulting in mixing between the two layers. During the transition to a turbulent regime, single and sometimes moving multiple cusps are observed around the periphery of jumps. A semi-empirical model is devised that relates the parameters of the laboratory experiment, i.e. flow rate, inlet nozzle radius, kinematic viscosity and reduced gravity, to the layer depth beyond the jump and the radius at which an undular jump occurs. The experiments imply that surface tension is not an essential ingredient in the formation of circular hydraulic jumps and demonstrate that stationary jumps can exist in stratified shear flows which can be represented as two discrete layers. No stationary circular undular jumps are found, however, in the case of a downward jet of dense fluid when the overlying, less-dense, fluid is stratified, but a stationary turbulent transition is observed. This has implications for the existence of stationary jumps in continuously stratified geophysical flows: results based on two-layer models may be misleading. It is shown that the Froude number at which a transition of finite width occurs in a radially diverging flow may be less than unity.

---

## 1. Introduction

### 1.1. *Background; jumps in single layers*

The circular hydraulic jump observed in a kitchen sink is a familiar phenomenon. The jump, or abrupt change in thickness of the flowing water, forms in the radial flow of a thin layer of water surrounding the point of impact of a jet of water (from a tap or faucet) directed vertically onto a smooth horizontal surface (the bottom of the sink). Typically the thin radially flowing layer is less than a millimetre in thickness

† Author to whom correspondence should be addressed at: ‘Bodfryn’, Glanrafon, Llangoed, Anglesey LL58 8PH, UK; oss413@sos.bangor.ac.uk

and the jump forms at a radius of a few centimetres from the vertical jet, increasing the water depth by a factor of order five or more.

Study of circular jumps has attracted much interest over the years since being mentioned by Rayleigh (1914) in a paper on hydraulic jumps and bores. Laboratory experiments and theoretical analyses of circular jumps are described by Watson (1964), Craik *et al.* (1981), Bowles & Smith (1992), Bohr, Dimon & Putkaradze (1993), Higuera (1994), Bush & Aristoff (2003) and Bush, Aristoff & Hosoi (2006). (The latter give further references.) Viscosity affects the thin radial flow and surface tension influences the character of the jump. Jumps of relatively small amplitude, in which the water depth does not change greatly in the transition, are often preceded by 3–5 stationary capillary waves and followed by a small but detectable change in surface slope, described by Craik *et al.* (1981) as an ‘outer ring’. Watson’s (1964) theory for the flow approaching a jump and for its location is in fair agreement with laboratory experiments and forms the basis of several subsequent studies, e.g. those of Higuera (1994) and of Bush & Aristoff (2003). (We shall later, in §3, adapt Watson’s theory to two layers.) The form of larger jumps is unstable, with temporally periodic fluctuations and sometimes with well-defined cusps around the periphery of the jump. Capillary–gravity waves are observed propagating downstream beyond the jump. Boundary layer separation and closed circulation cells or ‘rotors’ are observed in the jump, the latter causing the surface slope change or the ‘outer ring’, and stable shapes other than circular are found to be possible. The more recent studies have used numerical techniques to model the flow, and experiments have been made with a variety of different fluids to test effects of viscosity and surface tension, together with high-speed video to track microbubbles and so to estimate flow speeds.

### 1.2. Jumps in two-layer flows

No comparable study appears to have been made of circular *internal* hydraulic jumps in either miscible or immiscible fluids. These are produced as a vertical downwards-going jet of fluid denser than that into which it is introduced spreads horizontally from its point of impact with a horizontal surface, or when an upward jet of relatively lower density spreads after meeting the free surface of its surrounding fluid. Examples of these internal jumps are shown in §2. In the miscible fluids described here and unlike the single-layer circular jump, surface tension is negligible, the way in which the velocity profile in the radially spreading flow is controlled by viscous drag differs (and differs also in the two cases of upward- and downward-going jets) and a feature of the jumps is that, when their amplitude (the ratio of the flowing layer’s thickness after and before the jump) is moderate, they are characterized by stationary circular waves; transitions with small depth change are undular in form.

Our purpose is to draw attention to the phenomenon, rather than to match the relatively sophisticated studies recently made of surface jumps. The subject of whether stationary internal hydraulic jumps can occur in a stratified flow beneath an unstratified stationary layer is of importance in relation to the jumps of much greater size that are postulated to occur in rapid flows through channels on the sides of mid-ocean ridges and through passages connecting deep ocean basins (Polzin *et al.* 1996; Thurnherr *et al.* 2005; Thorpe 2007). Such flows, for example of the Antarctic Bottom Water through the Romanche Fracture Zone, are separated by relatively intense density gradients from the slow movement and low stratification of the overlying water. It is possible that the mixing observed downstream of sills in the passages is caused by stationary jumps, although there are as yet no observations with sufficient resolution to establish the presence or otherwise of such transitions.

In some circumstances the theory of jumps in inviscid two-layer flows is almost identical to that in a single layer and the occurrence of circular interfacial jumps is therefore not unexpected. In a two-layer flow, with the lower layer of thickness  $h$  and density  $\rho_2$  in uniform motion,  $u$ , beneath a deep stationary fluid of density  $\rho_1$  ( $\rho_1 < \rho_2$ ), long internal waves move relative to the lower layer at a speed,  $C = (g'h)^{1/2}$ , where  $g'$  is the reduced gravity,  $g' = g(\rho_2 - \rho_1)\rho_2$ , which, remarkably, is the same as that of waves on the interface when the lower layer is at rest (Appendix: A 1). There are two possible speeds for long waves: one downstream relative to the flow, the other upstream. The speed of these waves relative to the upper stationary layer are  $(u + C)$ , corresponding to a wave moving downstream relative to the flow, and  $(u - C)$ , a wave propagating against the flow. If the Froude number,  $(u/C)^2$ , is greater than 1, the second wave has a positive downstream speed,  $(u - C) > 0$ , between that of the lowest flow speed – which is zero (the speed of the upper layer) – and that of the lower layer. This wave therefore travels at speeds within the range of those in the mean flow. Since the long waves are the fastest moving and because the group velocity of long waves is equal to the phase speed,  $C$ , and is less than  $C$  for waves of smaller length, all linear waves and their wave energy must propagate downstream. No wave energy from a region of a stationary transition in a flow with Froude number  $> 1$  can propagate or change the flow upstream of a transition. Downstream of a transition where the Froude number is less than 1, long waves can travel both towards and away from the transition. These are conditions usually found as necessary for hydraulic jumps to occur and, in particular, are those found in relation to jumps in single-layer flows.

### 1.3. Jumps in stratified flows

Whilst jumps in naturally occurring stratified fluids are commonly represented as being at the interface between two uniform layers (e.g. see Baines 1995; Holland *et al.* 2002; Hassid, Regev & Poreh 2007), in reality flows are generally continuously stratified with no discontinuities in either density or velocity. In such shear flows, waves (and waves are intimately related to the presence or absence of hydraulic jumps as explained above) have properties that differ from those in two layers. For example, inviscid two-layer flows with non-zero velocity difference are unstable since wave disturbances can be found that, if sufficiently short, will grow through Kelvin–Helmholtz instability but, by the Miles–Howard theorem, in a continuously stratified flow instability is only possible when the smallest gradient Richardson number in the flow,  $Ri_{min}$ ,  $< 1/4$ . Because of the critical layer phenomenon in continuously stratified shear flow, contrary to what is described above at a Froude number  $> 1$  in a two-layer flow, waves cannot travel with a horizontal phase speed within the range of the mean flow.

The definition of an appropriate Froude number in a stratified shear flow requires some discussion. An appropriate choice is one that provides information about the propagation of wave energy in a direction contrary to the flow measured relative to a transition. Here the transition is supposed to be stationary. Let us assume, as in Thorpe & Ozen (2007), that a stratified layer with unidirectional velocity,  $U(z)$ , and density,  $\rho(z)$ , lies beneath a static layer which is at rest (a case that approximates to that of the circular hydraulic jump). A suitable measure, and one consistent with that in single-layer hydraulic theory, is the square of the mean downstream velocity,  $\langle u \rangle$  in the flowing layer divided by the square of the greatest group velocity in the upstream direction measured relative to the mean downstream velocity,  $Fr = \langle u \rangle^2 / (\max(C_g))^2$ . If  $Fr$  exceeds 1 then no waves can transmit energy upstream from the stationary transition. For reasons given later in §1.3, in some stratified shear flows  $Fr$  may always be less than unity. It is evident that, in choosing and applying this definition,

both the speed of the flow over the ground and the speed of a transition must be taken into consideration. The spatial variations in flow speed and stratification resulting from the radial flow approaching a circular jump add further complexity that is not present in unidirectional flows.

When the smallest gradient Richardson number in the flow,  $Ri_{min}$ , exceeds  $1/4$  this conclusion is consistent with Bell's (1974) study of the range of speeds of internal waves: waves must either travel at speeds,  $C$ , greater than the maximum in the flow,  $u_{max}$ , or less than the minimum flow speed,  $u_{min}$ . When a stratified layer has a velocity that is everywhere downstream and lies beneath a stationary layer of uniform density (so excluding the possibility of internal wave radiation upwards from disturbances in the lower layer) the condition  $C < u_{min}$  implies that waves may travel with negative velocity and so upstream, because  $u_{min} = 0$ . Long internal waves propagate faster than those of finite length and (like long surface waves) their group velocity is equal to their phase speed. An example in which long waves can travel upstream, whatever the magnitude of a specified mean flow in a fluid with two layers of uniform density, is given in Appendix A 2. Instability is not assured by the Miles–Howard theorem when  $Ri_{min} < 1/4$ ; some inviscid flows with  $Ri_{min} < 1/4$  that are close to a plane horizontal boundary are stable to small disturbances. Long waves are found in such flows that can propagate and transport energy upstream, although at speeds small compared to the greatest speed within the moving lower layer (Thorpe & Ozen 2007). Whether jumps can then occur is uncertain, but appears unlikely.

Observational evidence is less than decisive. There seem to be no experiments in which stationary jumps are formed in continuously stratified unidirectional flows over a rigid boundary but where the motion is zero at some height above the boundary. Wilkinson & Wood (1971) report a laboratory experiment in which a stationary jump appears to occur in a miscible two-layer flow just downstream of the entry of an upper heated (and therefore less dense) layer into a tank of stationary, colder (denser) water. (For experimental convenience this is the inverse of that described earlier. In Wilkinson & Wood's experiment, it is the relatively thin *upper* layer that is in motion, but in the Boussinesq approximation this is equivalent to the case where the lower layer is in motion.) The upper layer is restricted or 'controlled' downstream by a broad-crested inverted weir. The interface between the layers descends gradually from close to the inlet (which prevents the possibility of upstream wave propagation), with no sign of internal waves but with evidence of mixing by small billows, before a region is reached containing a 'roller' but where there are no signs of overturning at the interface and where, indeed, there is little or no further entrainment of fluid across the now indistinct interface. The roller does not have a form with a change in interface level like the hydraulic jumps observed in single layers downstream of weirs or in tidal bores. It seems possible that the transition and mixing observed may be a consequence of Kelvin–Helmholtz shear instability as in the laboratory experiments of Brown & Roshko (1974), rather than a hydraulic jump or transition. The persuasive image of what is described as a stationary internal hydraulic jump in the lee of the Sierra Nevada range in the books by Turner (1973; his figure 3.11) and Lighthill (1978; his figure 117) is attributed by Scorer (1972) to flow separation ahead of a rotor within the leading wave of train of large internal waves, but appears, nevertheless, to be a stationary flow transition.

The conditions in which stationary hydraulic jumps may occur in stratified flows are therefore not entirely clear. The present study shows that stationary undular jumps can exist in the flow of two miscible fluids when, by analogy with single-layer flows and as discussed in § 1.2, hydraulic jumps are indeed expected. When, however, the stratification is continuous (when the overlying, stationary and less-dense layer

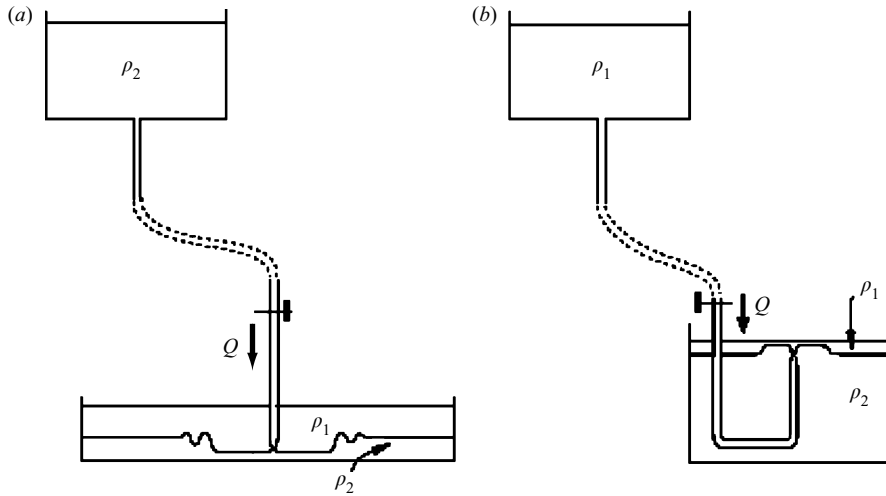


FIGURE 1. Apparatus for (a) the downward-going jet and (b) the upward-going jet. At the top, well above the lower tank, is a header tank filled of (a) saline water ( $\rho_2$ ) or (b) fresh water ( $\rho_1$ ). This tank is connected by a tube, with a tap to control and set the flow rate,  $Q$ , to the lower tank where the circular jumps are produced. In some experiments, the header tank is replaced by an adjustable-speed pump to set the flow rate. The fluid passes through a vertically pointing nozzle (a) downwards in fresh water contained in the lower square tank or circular pie dish, or (b) upwards in saline water. Visualization is provided by colouring the fluid introduced into the lower tank and, in (a), by shadowgraph.

is stratified), a further experiment described in §5.2 shows that stationary undular jumps do not form, but a turbulent transition is observed.

#### 1.4. Content and arrangement

The two-layer experiments are described in §2 and a theoretical model relating to the radial position of the jump is developed in §3. (Details of the model are given in Appendix C.) The experimental results are compared with the model in §4. Conclusions are discussed in §5, together with the results of the experiments referred to above in which a diffuse interface is inserted above the lower fluid to make the stratification continuous. A note on the Froude number required for a transition of finite width in a two-layer radial flow is presented in Appendix D pointing to effects associated with curved jumps.

## 2. Experiments

The apparatus is sketched in figure 1. Initial experiments (figure 1a) were made in a 1 m square Perspex tank. Subsequent experiments were made in a 58.4 cm square tank with a glass bottom, or in a circular Pyrex container (a pie dish) with a base of radius 9.35 cm placed within the 58.4 cm tank into which fluid could overflow. Preliminary results are given in Kavčič (2008). The tanks are first filled with fresh water of density  $\rho_1$  to a depth of 30–50 mm or enough to completely submerge the 35 mm deep pie dish when it is used, and left to settle for at least 10 min. Salt solution of density  $\rho_2$ , where  $(\rho_2 - \rho_1)/\rho_2 \approx (0.05\text{--}0.1)$ , is then introduced at a constant rate,  $Q$ , through a vertical tube terminating in a downwards pointing nozzle of radius  $a$ , at a height of about 0.3 cm from the horizontal base of the tank. (The height is kept small to avoid mixing between the descending fluid and that surrounding it.) Although larger nozzle radii were tried, the steadiest jumps were obtained with  $a \approx 1$  mm. Flow rates,

$Q$ , range from 0.398 to 7.42 cm<sup>3</sup> s<sup>-1</sup>. The Reynolds number of the flow,  $U_0 = Q/\pi a^2$ , through the nozzle is  $Re = U_0 a/\nu = Q/\pi a \nu$ , where  $\nu$  is the kinematic viscosity, and ranged from 112 to 1790 (an order of magnitude less than in Watson's experiments in a single layer – he defines  $Re$  as  $Q/a\nu$ ), and sufficiently small for the flow through the inlet tube to be laminar. The reduced gravity,  $g' = g(\rho_2 - \rho_1)/\rho_2$ , has values of about 50 and 100 cm s<sup>-2</sup>.

The diverging flow of the dense saline fluid over the base of the tank takes the form of a density current that spreads radially from the nozzle to the tank walls in a time depending on the reduced gravity  $g'$ , the flow rate and the tank dimensions, but typically 30–100 s. Reflected waves return on the interface between the fresh and saline layers towards the centre of the tank, but a relatively steady state of outward radial flow is set up after a minute or so, the larger times corresponding to larger tanks and to smaller  $Q$  or less-dense saline injections. At an early stage, often whilst the spreading density current is still visible, a circular undular jump forms at the interface between the saline fluid and the fresh water at distances from the nozzle of about 10–50 mm. No evidence of growing disturbances or Kelvin–Helmholtz billows is seen in the radially divergent flow approaching the jump.

Close to the location of the nozzle, the thickness,  $h$ , of the layer of dense water spreading radially on the bottom of the tank could not be directly measured but appeared to be less than 1 mm. Because of the continued influx,  $Q$ , into the finite container, the depth of the layer of dense water downstream of the jump slowly increases in time. Its mean depth,  $\langle h_2 \rangle$ , can be estimated as  $Qt/A$ , where  $t$  is the filling time and  $A$  the area of the tank outside the jump, and ranges during experiments from about 0.3 to 8 mm.

Photographs of the jumps were taken at periods sufficient to record the main changes apparent in the slowly varying flow patterns, every 30 s or less. In the first experiments jumps were made visible by using potassium permanganate to dye the saline water and colour filters were used to enhance contrast in the photographic images. Figure 2 shows a series of photographs taken in the 1 m square Perspex tank, with  $Re = 783$  as the mean depth,  $\langle h_2 \rangle$ , gradually increased. In figure 2(a) three stationary dark bands, indicating stationary wave crests where the thickness of the saline water is increased, are formed around the inlet. The innermost wave appears as a dark band and is one of elevation; the depth of the dye layer is increased. The innermost circular band appears darker than those of greater radii and darker than the surrounding layer beyond the jump, suggesting that the layer in the band is deeper than the surrounding layer. The distance between successive waves, their wavelength, is roughly 5 mm but decreases with increasing distance from the nozzle, a feature that is shown in § 3.1 to be a condition for interfacial waves to be stationary in a flow that decreases in speed as radius increases. The transition from the interior flow, before it reaches the inner dark ring, to the exterior region of relatively uniform shade of darkness and therefore uniform thickness, occurs between radii of about 16 mm and 30 mm.

As time and  $\langle h_2 \rangle$  increase the radius at which the jump occurs decreases slowly. After a few minutes, the waves lose their perfectly circular form, with evidence of patches of azimuthal undulations around the periphery of the jump with wavelength comparable to that of the circular waves. These are already seen in the top right quadrant of figure 2(a). They become more cusp-like, the radius of the jump decreases, and the width of the transition and number of visible waves decreases; the abrupt jumps, without waves, that eventually develop have radii that are less than the radii at which the undular jumps are observed. In some cases, e.g. figure 3(d), the pattern

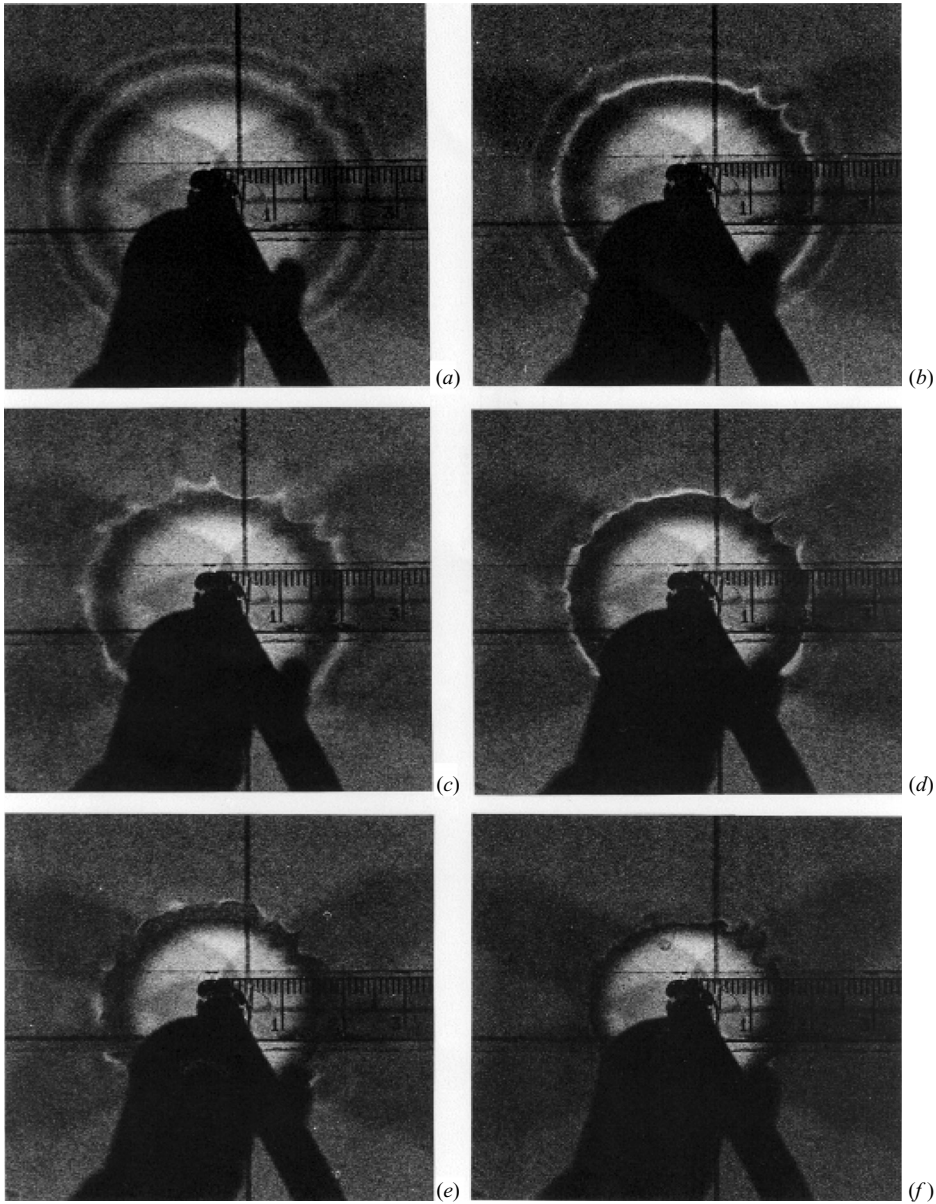


FIGURE 2. The circular internal hydraulic jump around a downward-going jet as in figure 1(a): a series of photographic images obtained using dye to colour the saline water as the thickness of the layer outside the jump gradually increases. The scale is in centimetres and the black silhouette in the lower part of the images is the entry tube and supports. The nozzle's radius is 1 mm and it is placed 3 mm from the floor of the 1 m square Perspex tank. The flow rate  $Q = 2.46 \text{ cm}^3 \text{ s}^{-1}$  with corresponding  $Re = 783$ , and the upper layer of water is 34 mm thick. The 'reduced' acceleration due to gravity is  $g' = g(\rho_2 - \rho_1)/\rho_2 \approx 104 \text{ cm s}^{-2}$ , where  $g$  (taken as  $981 \text{ cm s}^{-2}$ ) is the acceleration due to gravity. Values of respective times, depths and parameters are listed in table 1.

of cusps is seen to rotate around the periphery of the jump, and this rotation indicates the beginning of a transition to turbulence. There is evidence of irregular turbulent motion around the circumference of the jump at the stages shown in figure 2(d-f). The

transition to an abrupt turbulent jump is accompanied by the outward propagation of interfacial waves.

Clearer images were subsequently obtained using shadowgraph images produced by shining a parallel beam of light upwards through the tank onto a transparent screen just above the fresh water layer. A ruler was placed on the screen, or lines and circles were drawn, to provide a scale.

Figure 3 illustrates the development of the jump in the 58.4 cm square tank when  $Re = 232$ . The first image, (a), is 20 s after filling with the dense fluid had begun, and a circular jump is already visible. The innermost circle is lighter, consistent with its being caused by a wave of elevation focusing light refracted as it passes upwards through a concave interface between the salt and fresh water; the bright bands are formed at wave crests and dark bands are the wave troughs. The density current reached the sidewalls of the tank after about 50 s, and by the time of (b), at 2:10 min after filling began, the dense layer surrounding the jump is well established and fairly steady. Three stationary waves are visible in (b) and two in (c), at 4:50 min, with radius decreasing in time. In (d) at about 6 min, a pattern of cusps or waves is formed, moving counter-clockwise around the inner stationary circular wave at a speed of roughly  $0.5 \text{ cm s}^{-1}$ . In (e) this pattern becomes unstable and begins to distort the stationary innermost wave, with evidence of small-scale turbulent structure that develops still further in (f, g), intruding into the region close to the nozzle. After about 14 min (h, i), the double ring pattern (possibly the boundaries of a rotor) surrounding the nozzle has a regular azimuthal pattern with a wavenumber of about 14 (i.e. with some 14 'cells' around the nozzle) but apparently in a less dynamic state of turbulence than at the transitional stages (f, g).

The images in figure 4 ( $Re = 1790$ ) are obtained in the 1 m square tank. The first image shows 3–4 near circular waves surrounding the inlet. The circular pattern is disturbed at bottom left by a feature seen in some other experiments. The single arrow-like protrusion develops a linear striation in (b) that breaks down into an eddying structure in (c). The image (b) shows the appearance of wisps or fine structure surrounding the ring, particularly at the upper right side, indicative of a transition to irregular motion. These become more evident in (c), but are not visible in figure 2. The multiple cusp-like features of figure 2 or figure 3(d) are not as evident in figure 4.

In some experiments dye was introduced into the flow in the hope of detecting the presence or absence of a rotor in the jump similar to that in single-layer jumps (remnants of the dye are visible in figure 3a, b), but these were inconclusive.

Values of the measured radii at the jump ( $r_1$ ), the mean depth outside the jump ( $\langle h_2 \rangle$ ), and the Froude number,  $Fr_2 = u_2^2/g'\langle h_2 \rangle$  for the experiments shown in figures 2–4 are given in table 1. The mean flow speed,  $\langle u_2 \rangle$ , is calculated from the volume flux,  $Q = 2\pi r_1 \langle h_2 \rangle \langle u_2 \rangle$  giving  $Fr_2 = Q^2/(4\pi^2 r_1^2 g' \langle h_2 \rangle^3)$ . The values of  $Fr_2$  are generally less than 1, as expected. There is some latitude in the definition of  $r_1$ , particularly when waves are present. Here it is taken to be the radius at which the onset of a rise in the interface is estimated to occur or  $r_w - \lambda/2$ , where  $r_w$  is the radius of the crest of the innermost wave and  $\lambda$  is its wavelength. This radius may be less than the radius at which the lower layer reaches the thickness  $\langle h_2 \rangle$  downstream of the transition, and this may be why some values of  $Fr_2$  in table 1 exceed 1. The value  $\langle h_2 \rangle$  may not however represent the value of the depth of the lower layer immediately downstream of the jump, a matter to which we return in § 3.1.



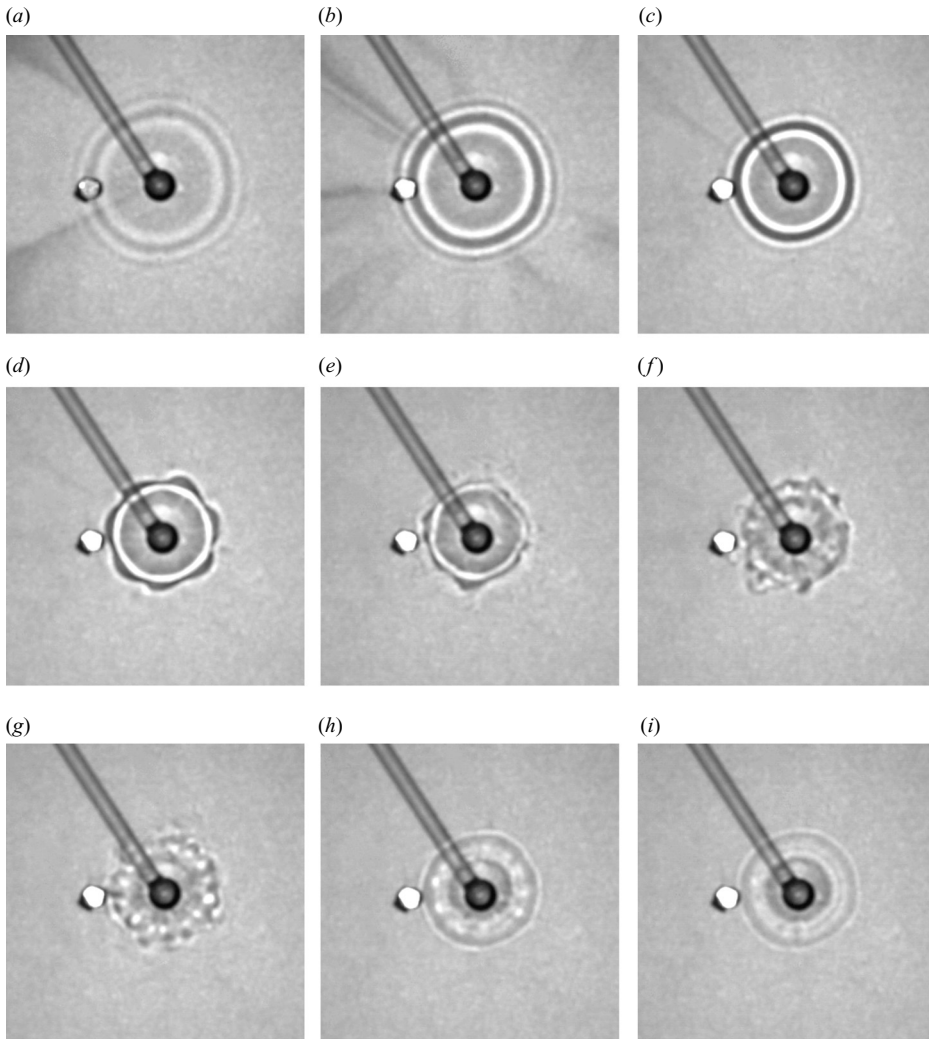


FIGURE 3. Patterns observed using shadowgraph in the 58.4 cm square tank at times after filling with the saline solution commenced of (a) 20 s, (b) 2:10 min, (c) 4:50 min, (d) 6:08 min, (e) 7:50 min, (f) 8:50 min, (g) 10:50 min, (h) 13:58 min and (i) 17:14 min. Here  $Q = 0.828 \text{ cm}^3 \text{ s}^{-1}$ ,  $Re = 232$ . The ‘reduced’ acceleration due to gravity is  $g' = g(\rho_2 - \rho_1)/\rho_2, \approx 48.8 \text{ cm s}^{-2}$ . The images are 7 cm square. The two dark lines from the top left to the centre are the sides of the filling tube. Dark streaks in (a) and (b) are potassium permanganate dye introduced through the circular hole to the left of the nozzle to visualize the flow. Parameters for (b–d) are listed in table 1.

A few experiments were made as shown in figure 1(b) with a jet of fresh water directed upwards through a nozzle towards the surface of a saline solution in a 65 cm diameter circular tank. These also resulted in the formation of waves and jumps. The irregular structure of the jump shown in figure 5 indicates that, as was observed, the transitions surrounding an upward-going jet spreading below a free surface are much less stable than that in a flow around a downward-going jet impinging on a horizontal rigid plane.

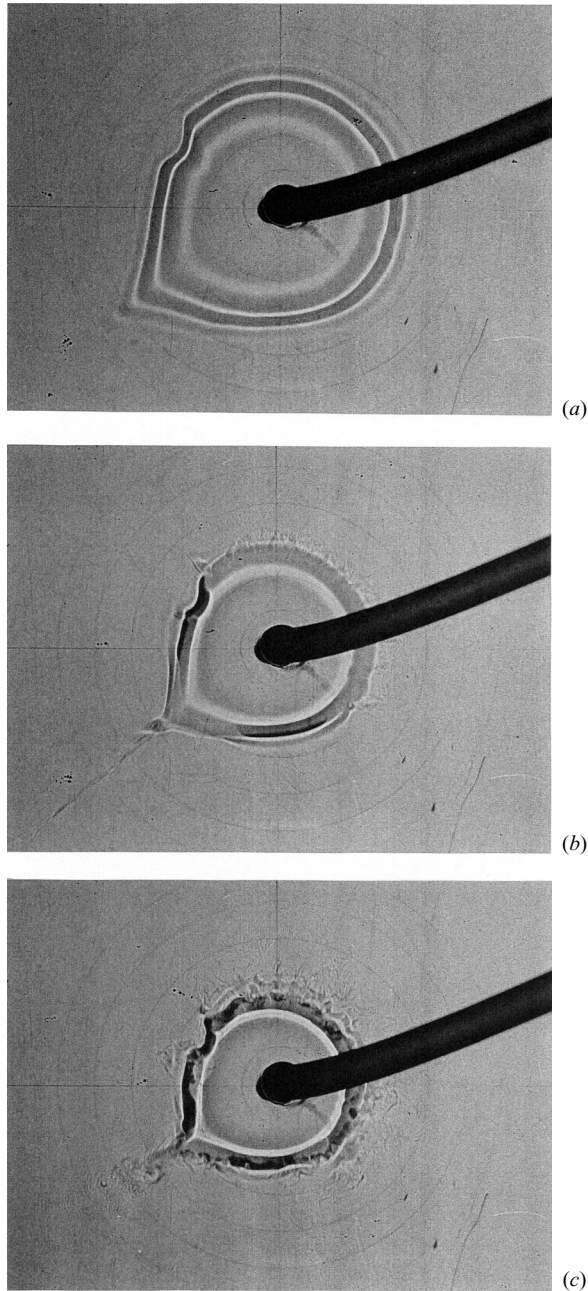


FIGURE 4. The circular internal hydraulic jump around a downward-going jet as in figure 1(a): images obtained using shadowgraph as the thickness of the layer outside the jump gradually increases. The nozzle's radius is 1 mm and it is placed 3 mm from the floor of the 1 m square Perspex tank. The flow rate  $Q = 5.63 \text{ cm}^3 \text{ s}^{-1}$  with corresponding  $Re = 1790$ , and the upper layer of water is 34 mm thick. The 'reduced' acceleration due to gravity is  $g' = g(\rho_2 - \rho_1)/\rho_2 \approx 98.8 \text{ cm s}^{-2}$ . Values of respective times, depths and parameters are listed in table 1. The images are 15 cm wide.

Figure	$t$ (min:s)	$r_1$ (cm)	$\langle h_2 \rangle$ (mm)	$Fr_2$	$h_2$ (mm)	$Fr_2(\lambda)$
2(a)	8:30	1.60	1.25	0.295	0.68	0.904
2(b)	11:0	1.45	1.62	0.156	0.75	0.835
2(c)	11:30	1.52	1.70	0.130	–	–
2(d)	12:30	1.37	1.85	0.124	–	–
2(e)	13:30	1.35	2.00	0.101	–	–
2(f)	15:30	1.25	2.30	0.078	–	–
3(b)	2:10	1.03	0.32	10.7	0.291	0.939
3(c)	4:50	0.92	0.70	1.20	0.294	0.919
3(d)	6:08	0.88	0.89	0.65	–	–
4(a)	7:0	2.00	2.35	0.157	1.10	0.750
4(b)	8:15	1.90	2.70	0.114	1.20	0.708
4(c)	10:0	1.90	3.40	0.072	–	–

TABLE 1. Values of the parameters of figures 2–4. In figure 2,  $Q = 2.46 \text{ cm}^3 \text{ s}^{-1}$  and  $g' = g(\rho_2 - \rho_1)/\rho_2$ , is about  $104 \text{ cm s}^{-2}$ . In figure 3,  $Q = 0.828 \text{ cm}^3 \text{ s}^{-1}$  and  $g'$  is about  $48.8 \text{ cm s}^{-2}$ . In figure 4,  $Q = 5.63 \text{ cm}^3 \text{ s}^{-1}$  and  $g'$  is about  $98.8 \text{ cm s}^{-2}$ . The columns are: figure number; the time after filling started ( $t$ ); the radius at the onset of the jump ( $r_1$ ); the mean depth outside the jump  $\langle h_2 \rangle$  estimated from  $Q$  and  $t$ ; the Froude number,  $Fr_2 = Q^2/(4\pi^2 r_1^2 g' \langle h_2 \rangle^3)$ , based on the depth  $\langle h_2 \rangle$ ; the depth,  $h_2$ , determined from the wavelength as in §3.1 using (3); and the Froude number,  $Fr_2(\lambda)$ , determined from (1). Gaps (–) occur where jumps are not undular, so that  $\lambda$  cannot be estimated.

### 3. Theory and a model

#### 3.1. Estimating $h_2$

Suppose the jump occurs at a radius  $r_1$  beyond which the flow speed,  $U_1$ , is uniform through the depth,  $h_2$ , of the lower layer and zero above. The depth  $h_2$  may be estimated from the filling rate, the time since filling begins and the tank area beyond the jump. However, since the radial flow speed in the region  $r > r_1$  beyond the jump must tend to zero at the sidewalls of the tank, the pressure must increase radially, and so must the depth of the lower layer. In quasi-steady conditions, the depth at the jump at  $r_1$  is therefore probably less than  $\langle h_2 \rangle$ . The values of  $Fr_2 \propto \langle h_2 \rangle^{-3}$  in table 1 may substantially underestimate the Froude number of the flow just downstream of the jump. An assessment of the magnitude of the underestimate is given in Appendix B.

An alternative estimate of the depth  $h_2$  at the jump,  $r = r_1$ , is available. With the assumption that the flow in the lower layer is uniform and equal to  $U_1$  beyond the transition at radius  $r_1$ , we use the fact that waves are stationary to estimate the depth of the layer,  $h_2$ . The condition that the upstream phase speed of the waves is zero gives a relation between the Froude number and  $kh_2$ ,

$$Fr_2 \equiv U_1^2/g'h_2 = (\tanh kh_2)/kh_2, \tag{1}$$

where  $kh_2 = 2\pi h_2/\lambda$ , and  $\lambda$  is the wavelength ((A 5), Appendix A 1). It follows that  $Fr_2$  must be less than unity. Using  $Q = 2\pi r h_2 U_1$ , we can write (1) as

$$Q^2/(4\pi^2 r^2 g' h_2^3) = (\tanh kh_2)/kh_2. \tag{2}$$

If  $h_2$  does not change with radius,  $r$ , it follows that, since the right-hand side of (2) decreases with increase in  $kh_2$ ,  $kh_2$  increases as  $r$  increases, and so the wavelength must decrease with increasing radius, as observed.

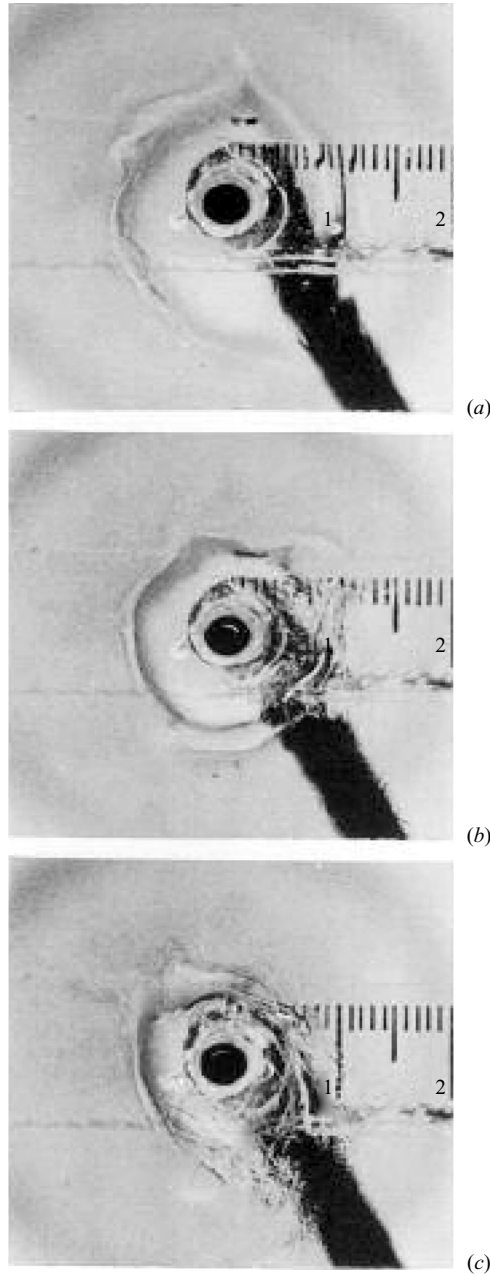


FIGURE 5. An example of an internal hydraulic jump around an upward-going jet of dyed water as in figure 1(b) ascending to the surface of a 190 mm thick layer of saline water with  $Q = 0.484 \text{ cm}^3 \text{ s}^{-1}$ ,  $Re = 154$  and  $g' = g(\rho_2 - \rho_1)/\rho_1 \approx 98 \text{ m s}^{-2}$ . The nozzle radius is 1 mm and it is placed 5 mm below the surface at the centre of a circular tank of 32.5 cm radius. The images are 4 cm square. The dark band from bottom right is the tube leading to the nozzle. Photos are taken at times (a) 5 min, (b) 7 min, and (c) 9 min after filling through the nozzle commenced, so that, based on the filling rate, the mean thickness of the upper layer,  $\langle h_1 \rangle$ , is 0.44, 0.61 and 0.79 mm, respectively.

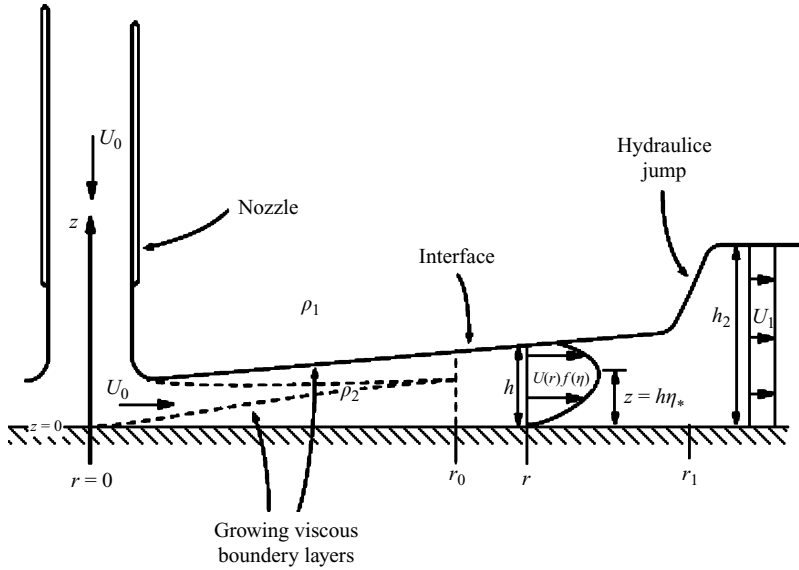


FIGURE 6. The radially spreading viscous layer. The boundary layers at the horizontal plane and at the interface combine at a radius  $r_0$ , beyond which there is a similarity solution for the radial velocity and layer depth,  $h(r)$ . The jump or transition occurs at radius  $r_1$ , and beyond this the flow,  $U_1$ , is assumed to be uniform in depth. Flows induced in the upper layer are relatively slow and have been disregarded.

Multiplying (2) by  $(kh_2)^3$  gives

$$x^2 \tanh x = \Phi, \tag{3}$$

where  $\Phi = 2\pi Q^2 / (r^2 g' \lambda^3)$  and  $x = kh_2$ . The values of  $Q$ ,  $r$ ,  $g'$  and  $\lambda$  contributing to  $\Phi$  can be determined from the experiments, so  $\Phi$ , and hence  $x$ , can be estimated from (3) at the mean radius  $r$  of a wave of length  $\lambda$ . The layer thickness,  $h_2$ , is then  $h_2 = \lambda x / 2\pi$ . The estimate depends however on the assumption that the mean flow where the waves occur is uniform through the layer and that curvature of the wave crests can be neglected. The latter will be valid provided the wavelength is much less than the radius at which the waves occur. The ratio of wavelength to radius in the experiments is, however, typically 0.3, so the assumption is at best dubious. The effect of shear in the layer may be assessed using the model described in Appendix A 2. The uncertainty in the estimate of  $h_2$  depends on  $\Phi$ . Typical values range from about 0.3 to 1.3, and values of  $h_2$  may be in error by  $\pm 50\%$ . The comparison of theory and observation must be viewed with this uncertainty in mind, as well as the effects of the other assumptions made. We test the sensitivity of a model of the jump to estimates of  $h_2$  in § 4.

### 3.2. The viscous flow at $r < r_1$

We suppose that the rapid shallow radial flow in the lower layer is strongly affected by the viscous stresses on its boundaries at radii less than  $r_1$  at which a jump occurs, but that in the slower flow at radii exceeding  $r_1$  viscosity is of less importance and the flow can be regarded as inviscid and irrotational. Figure 6 is a sketch of the supposed development of the flow with distance,  $r$ , from the location where the vertical jet meets the horizontal plane. Following Watson (1964) we suppose the lower layer of density  $\rho_2$  is of thickness  $h(r)$  at radius  $r$  from the nozzle as it approaches the jump. The flow in the layers will be affected by the presence of viscous stresses at the underlying

horizontal plane and at the interface between the layers. We shall neglect the effects of diffusion of salt across the interface since the molecular diffusion coefficient,  $\kappa_S$  is about  $1.4 \times 10^{-5} \text{ cm}^2 \text{ s}^{-1}$ , and is much less than the coefficient of molecular viscosity,  $\nu \approx 10^{-2} \text{ cm}^2 \text{ s}^{-1}$ ; over the radial distance taken for the flow to reach the transition, the flow in the lower layer will affect that in the upper through viscous forces, but the layers will remain almost uniform in density.

Details of the procedure used to estimate the flow in the lower layer are given in Appendix C1. The analysis supposes that very close to the nozzle the flow in the lower layer is uniform and equal to  $U_0$ , but with increasing radius the effects of the viscous stresses at the horizontal lower boundary and at the interface with the upper layer spread vertically, reducing the momentum of the flow. The effects extend throughout the depth of the lower layer at a distance  $r_0$  from the nozzle when the two boundary layers merge as sketched in figure 6. Beyond this radius a self-similar solution of the form

$$u = U(r)f(z/h) \quad (4)$$

is found, where  $U$  is the maximum horizontal speed in the layer and  $0 \leq f \leq 1$ . The non-dimensional function,  $f$ , satisfies the equation  $f'' = -3c^2 f^2/2$  with a non-dimensional constant  $c$ , and  $f(0) = 0$  to satisfy the no-slip boundary condition at the horizontal plane at  $z = 0$ . The maximum flow is at a level  $z/h = \eta_*$  where  $f(\eta_*) = 1$ . The solution for  $U$  is

$$U(r) = 2c_1^2 Q^2 / [c^2 \nu (r^3 + l^3)] \quad (5)$$

and

$$h(r) = c^2 \nu (r^3 + l^3) / [2Qc_1 r] \quad (6)$$

where  $l$  is a length, and  $c$  and  $c_1$  are constants such that ((C8) in Appendix C)

$$c \approx 2.804 - \int_0^{f(1)} (1 - f^3)^{-1/2} df \quad (7)$$

and (C9)

$$c_1 \approx c \left[ 1.725 - \int_0^{f(1)} f(1 - f^3)^{-1/2} df \right]^{-1}. \quad (8)$$

The maximum speed,  $U$ , decreases with  $r$ , and the layer thickness,  $h$ , decreases to a minimum at  $r = 2^{-1/3}l$  and then increases monotonically. The height at which the flow reaches its maximum value is given by (C7a):

$$\eta_* \approx 1.402c^{-1}. \quad (9)$$

### 3.3. The radius, $r_2$ , at the jump

Entrainment from the upper to the lower layer at the jump is disregarded, as is mixing at the interface; the lower layer is assumed to maintain its uniform density  $\rho_2$ . Conservation of momentum at the transition is expressed as equality between the net downstream force due to pressure and the rate of increase in the momentum at the transition, with the addition of any momentum lost by friction on the bottom in the transition region or lost through a flux of momentum downstream (as expressed in (C14) Appendix C2). The latter may be a result of transport in interfacial waves. Using (4)–(6) to describe the flow approaching the jump, the equations of conservation of volume and momentum flux at the jump lead to an equation (C19):

$$Y = Z, \quad (10)$$

where

$$Y = r_1 h_2^2 g' / (\nu \pi Re)^2 + a^2 / (2\pi^2 r_1 h_2) + M,$$

and

$$Z = \{8\pi c_1^3 Re / (3c^3 [(r_1/a)^3 + (l/a)^3])\} [1 - f'(1)/c] \\ + g' a^4 c^4 [(r_1/a)^3 + (l/a)^3]^2 / (4\pi^4 r_1 \nu^2 c_1^2 Re^4),$$

provided that  $r_1 > r_0$ , where  $Re = Q/(\pi a \nu)$ ,  $M = 2r_1 a^2 m / Q^2$  and  $\rho_2 m$  is the loss of momentum flux at the jump as a consequence of viscous stress at the boundaries of the moving layer and downstream radiation in the interfacial waves.

Watson finds that the radius,  $r_0$ , at which the bottom boundary layer extends to the top of a spreading single layer, is approximately  $0.4621a Re^{1/3}$ . Since in the two-layer flow there are growing boundary layers at both the upper and lower boundaries, a smaller value of  $r_0$  may be anticipated. The smallest observed value of  $r_1$  is  $0.878a Re^{1/3}$ , and we therefore assume that  $r_1 > r_0$  and that (10) is valid. The terms  $r_1$ ,  $h_2$ ,  $Re$ ,  $g'$  and  $a$  in (10) can all be estimated from the experiments. The constants  $c$  (7),  $c_1$  (8) and  $f'(1) = -c(1 - f(1)^3)^{1/2}$  (C6b), all depend only on  $f(1)$ ; the integrals in the expressions for  $c$  and  $c_1$  can be evaluated numerically once a value for the unknown,  $f(1)$ , is specified. From (C13) we may write  $l/a = q Re^{1/3}$ , where  $q$  is a second unknown constant. The non-dimensionalized momentum loss,  $M$ , is likely to be proportional to the square of the amplitude of the interfacial waves and to the kinematic viscosity, but without further information we shall suppose it is constant. The unknown quantities in (10) are therefore  $f(1)$ ,  $q$  and  $M$ . If they can be found, (10) provides an equation from which, in principle, the radius,  $r_1$ , at which the jump occurs can be found provided some means of estimating  $h_2$  is available.

The above analysis depends on several approximations and assumptions about the growth of the boundary layers and the nature of the transition (all described in Appendix C), but given the generally favourable comparison between Watson's theory and his laboratory measurements of jumps in a single layer, it appears that the analysis may provide a suitable framework within which to analyse the two-layer experiments.

#### 4. Estimates of the model constants from the laboratory data

Empirical 'best fit' values for the three unknowns,  $f(1)$ ,  $q$  and  $M$ , are determined by inserting a set of trial values into the expression  $(Y - Z)$  evaluated using data from 15 experiments in periods when undular jumps are observed. Data are taken at times after the dense layer has spread as a density current to the container boundaries and after the time at which any reflected disturbances have reached the nozzle location. Each experiment provides between 1 and 4 sets of values of the measurable terms, giving sets of values to optimise the solution of (10). The trial values that give the minimum sum of  $(Y - Z)^2$  are taken as the best estimates of the unknowns.

Figure 7(a) shows  $Y$  plotted against  $Z$  with the best fit values of  $f(1) = 0.910$ ,  $q = 0.840$  and  $M = 2.15 \times 10^{-3}$ , giving  $c = 1.754$ ,  $c_1 = 0.2319$ ,  $f'(1) = -0.870$  when the wavelength of the innermost internal waves is used in (3) to estimate  $h_2$ . The data from the experiments give 34 sets of measured values and collapse fairly well onto the straight line,  $Y = Z$ , with increasing values of  $Y$  and  $Z$  as  $Re$  decreases and  $g'$ , increases. The r.m.s. (root mean square) value of  $(Y - Z)$ , a measure of the scatter of the data about a linear fit, is equal to  $1.34 \times 10^{-3}$ . There is no apparent effect of tank shape or size; at the same value of  $a$ ,  $Q$  and  $g'$ , waves of the same wavelength (and therefore  $h_2$ ) are found at the same jump radius in the small pie dish and the 0.584 m

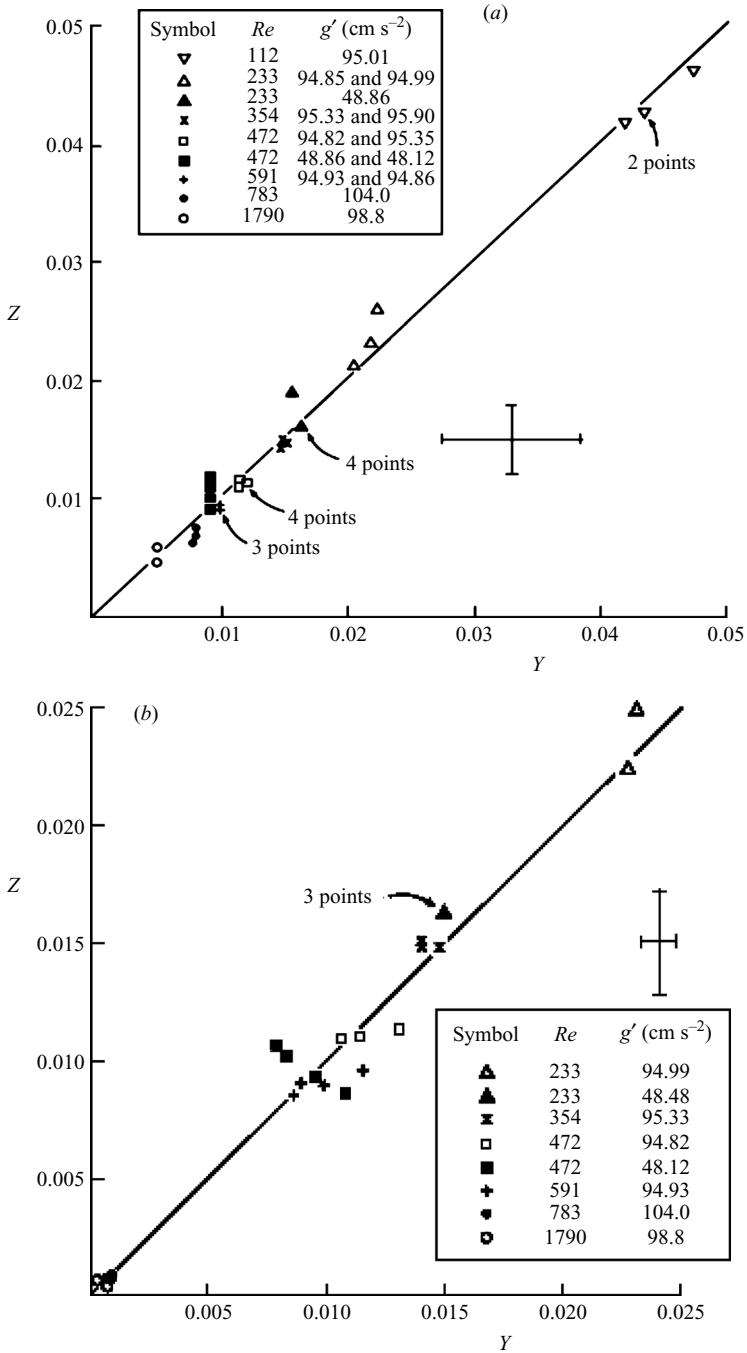


FIGURE 7. The variation of  $Y$  and  $Z$  given by equation (10) with optimal values of  $f(1)$ ,  $q$  and  $M$  given in the text with (a)  $h_2$  derived from (3) using the wavelength of the stationary waves and (b)  $h_2$  derived from the filling rate,  $Q$ . The symbols correspond to different values of  $Re$  and  $g'$  as shown. ‘Worst case’ error bars are indicated for points with  $Re = 354$ . Errors in  $Y$  arise mainly from possible uncertainty in the values of  $h_2$  in (a) (40%) and in  $r_1$  in (b) (7%), whilst worst case errors in  $Z$  (20%) are dominated by uncertainty in  $r_1$ .



square tank so  $h_2$ , is independent of the tank dimensions. The height,  $\eta_* = z/h$ , at which the greatest velocity occurs in the thin radially spreading dense layer is given by (9):  $\eta_* \approx 0.80$ .

The relatively small value of  $M$  indicates that, except at the higher values of  $Re$ , the rate of loss in momentum flux through wave radiation or viscous stress is small. In dimensional terms this flux is given by

$$\rho_2 m = 1.07 \times 10^{-3} \rho_2 Q^2 / r_1 a^2. \quad (11)$$

If this is due entirely to the waves, and if the wave stress is of order  $\rho_2 \langle uw \rangle h_2$  ( $\rho_2$  times the vertically integrated mean product of the horizontal and vertical velocity fluctuations), it follows that  $m = O(\langle uw \rangle h_2)$ . Equation (11) then leads to values of  $\langle uw \rangle^{1/2}$  that are of the same magnitude as the vertically uniform speed  $U_1$  downstream of the jump (e.g.  $\langle uw \rangle^{1/2} / U_1 \approx 0.43$  and  $0.98$  when  $Re = 233$  and  $1790$ , respectively). Velocity fluctuations that are comparable to the mean flow are indicative of conditions in which rotors may occur.

The collapse of the laboratory data using the determined values of the unknown quantities onto a straight line appears to imply that numerical solution of (10) provides a consistent model. However, in spite of evidence in the experiments to the contrary, values of  $q = h_2/h_1$  found using values of  $h_1$  given by (6) are, in many cases, less than unity and  $Fr_1$  is sometimes less than unity. The mean estimate of  $q$  is  $0.830$  and of  $Fr_1$  is  $1.66$  (but dominated by a single outlying value of  $16.14$ , the removal of which decreases  $Fr_1$  to  $1.22$ ). Whilst values of  $Fr_1 < 1$  may be possible as argued in Appendix D,  $q < 1$  appears unphysical. Moreover if  $h_2$  is determined from the wavelength of the waves, (10) includes two ‘unknowns’,  $h_2$  and  $r_1$ , and even with the determined empirical values of  $f(1)$ ,  $q$  and  $M$  cannot alone provide a means of predicting the radius,  $r_1$ , of the jump.

The radial location of an undular jump must depend on the ‘external measures’,  $a$ ,  $Q$  (or  $Re$ ),  $g'$ ,  $\nu$ , the tank geometry and the time,  $t$ , for which the tank has been filled. We can estimate  $\langle h_2 \rangle$  from  $Q$ ,  $t$  and the tank dimensions, and use this in the optimization of (10), together with the other values. Fits using data from the small circular pie dish are generally poor, possibly because of the relatively rapid deepening of the layer and the consequent rapid changes in the nature of the jump and its location, but the collapse of data from the larger square tanks is better. The best-fit values from eight experiments (24 sets of values) are  $f(1) = 0.950$ ,  $q = 0.980$  and  $M = 1.05 \times 10^3$ , giving  $c = 1.66$ ,  $c_1 = 0.2365$ ,  $f'(1) = -0.628$  and  $\eta_* \approx 0.84$ . The fit of  $Y$  to  $Z$  is shown in figure 7(b). The r.m.s. value of  $(Y - Z)$  is equal to  $1.34 \times 10^{-3}$ , coincidentally equal to the value for figure 6(a). Remarkably, the empirical values do not differ greatly from those obtained from data with  $h_2$  derived from (3). Values of  $q = \langle h_2 \rangle / h_1$  and  $Fr_1$  are shown in figure 8. There is considerable scatter and some values of  $q$  and  $Fr_1$  are less than unity (again see Appendix D), but there is some indication that  $Fr_1$  increases with  $q$ . Values of  $\langle uw \rangle^{1/2} / U_1$  are similar to those found using  $h_2$  derived from (3) (e.g.  $\langle uw \rangle^{1/2} / U_1 \approx 0.44$  and  $1.03$  when  $Re = 233$  and  $1790$ , respectively), again favouring rotor formation.

## 5. Discussion and further experiments

### 5.1. Discussion

Circular internal jumps occur when a thin layer of fluid spreads radially beneath (or above) a relatively deep layer of less (or more) dense, miscible fluid. In the case of a less-dense layer spreading on the surface of a deep dense layer shown in figure 5,

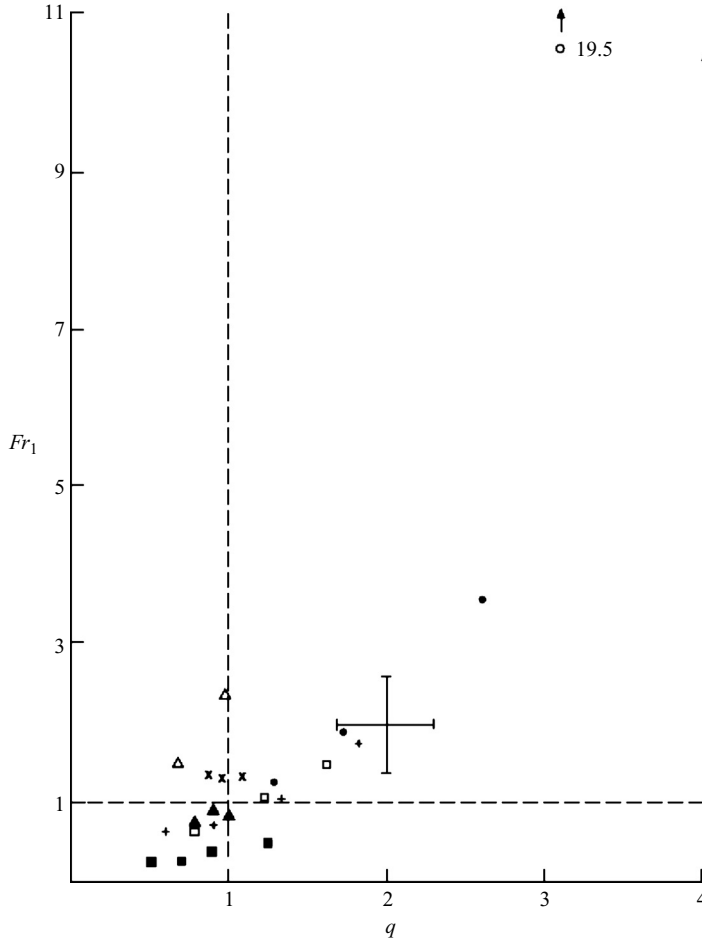


FIGURE 8. Values of the jump amplitude,  $q = \langle h_2 \rangle / h_1$ , and the Froude number of the flow approaching the jump,  $Fr_1$ , derived from experimental data incorporated into the model described in Appendix C 2. Symbols are as shown in figure 7(b). Error bars at  $q = Fr_1 = 2$  are shown assuming no error in estimates of  $c$  and  $c_1$ .

jumps are relatively unstable. This study has focused on the more stable jumps in dense saline layers spreading on a horizontal surface beneath fresh water.

This method of producing internal jumps provides a relatively simple means of studying their properties in closely controlled conditions. When first formed in a container of limited extent, the jumps are undular in form. As the thickness of the surrounding layer increases, the radial distance from the injection point at which jumps occur decreases, and the jumps become more abrupt with evidence of turbulence. The circumferences of the jumps observed during the transition from an undular and laminar form to one that is abrupt and turbulent are sometimes indented by azimuthal waves or cusp-like features with an appearance similar to the cusp/lobe structures observed at the head of a density current (Simpson 1997). Rotors were not detected in the experiments, but may have been present in the transition region. The absence of surface tension demonstrates that it is not an essential factor in the formation of all classes of circular hydraulic jumps, but viscosity does have an effect, at least on the properties of the flow between the inlet and the jump. The variations and irregular

flows observed in the presence of a free boundary in the inverted, less-stable case (figure 5) suggests that viscosity may affect the stability of jumps.

Numerical solution of (10), the equation derived from the model, with the empirically determined values for the unknown constants and the input of measured values, offers a means to predict the approximate radius at which an undular jump will occur. The model is unsatisfactory because no consideration is given to the motion of the upper layer of density  $\rho_1$ , a feature that should be addressed in a more thorough investigation through which, for example, an analytical value of  $f(1)$  might be derived and a more sophisticated model of the transition developed.

The presence of a pattern of circular internal waves, a circular undular jump, is in contrast to the relatively abrupt circular jumps observed in single-layer flows. The difference appears to be because, in the single layer, waves are affected by surface tension. The group velocity of relatively long gravity waves observed in undular bores in rivers is less than the phase speed; consequently energy is transmitted downstream by the stationary waves. However, the group velocity of short two-dimensional capillary-gravity waves, those of length less than 1.7 cm on a clean free surface not affected by surface-active contaminants, exceeds the phase speed. If the dynamics of the circular jump were controlled by short stationary waves – capillary waves – their energy would be directed upstream, modifying the approaching flow as noted by Craik *et al.* (1981).† Instead a finite-amplitude abrupt jump is formed. In the two-layer flow, surface tension is absent and the group velocity of waves is less than the phase speed, so the energy of stationary waves is transmitted downstream. In this sense, although these arguments disregard the effects imposed by the radial flow, the two-layer circular jump is more closely analogous to an undular bore in a river than to a small-scale circular jump in a single layer.

Craik *et al.* measured the changing height of the water surface across circular jumps in single-layer flows. The depth rises rapidly at the beginning of the jumps, the slope of the water surface decreasing to zero over distances of typically 0.4 times the radius of the jump. The equation of conservation of momentum in a jump of finite width in a radial flow differs from that in channel flow, and may lead to a critical Froude number that is less than unity, as explained in Appendix D. Bohr *et al.* (1993) remark that radial momentum is not conserved, and that ‘even though radial momentum is not conserved during the flow, it is still continuous across the’ (circular) ‘jump’, taken to be a flow discontinuity of zero width. But, as applied in Appendix D, momentum is directional, whilst ‘radial momentum’ is not. In a more general context, the analysis suggests that curvature of jumps, a feature common in the natural environment, may change the conditions for transition in ways not represented in two-dimensional jumps.

### 5.2. Experiments in continuous stratification

Two experiments were made, intended to test the conjecture expressed in §1.3 that stationary jumps may not occur in continuously stratified shear flows beneath a static layer. A dense bottom layer with an approximate thickness of 3.6 mm was produced by passing saline water through the nozzle for a short period into the 9.35 cm radius

† The capillary waves observed by Craik *et al.* (1981) upstream of the change in water level identified as a jump appear to be akin to those formed in the ‘Fish-line problem’ (Lamb 1932, para 272) or the parasitic capillaries found ahead of the crest of short surface gravity waves (Longuet-Higgins 1992 Duncan *et al.* 1999), but seem to play, at most, only a minor part in the dynamics of the jump.

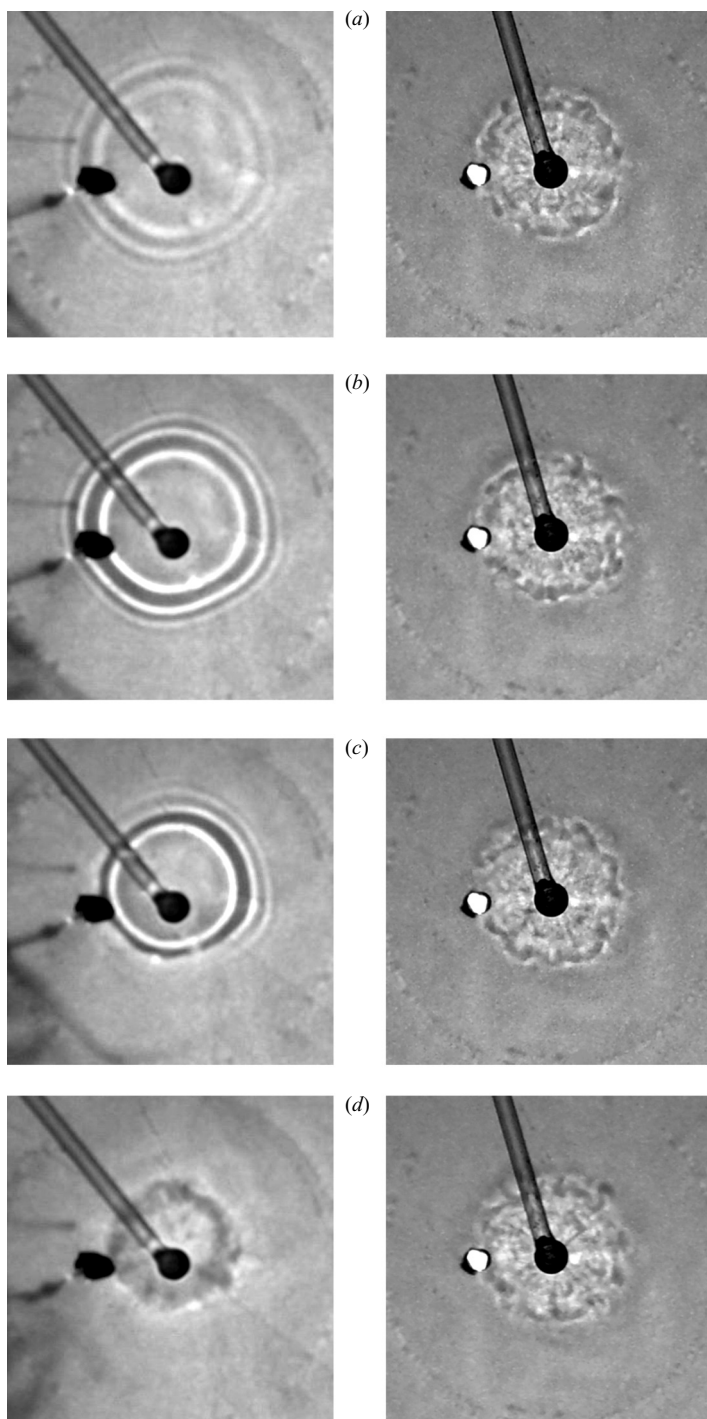


FIGURE 9(a-d). For caption see the facing page.

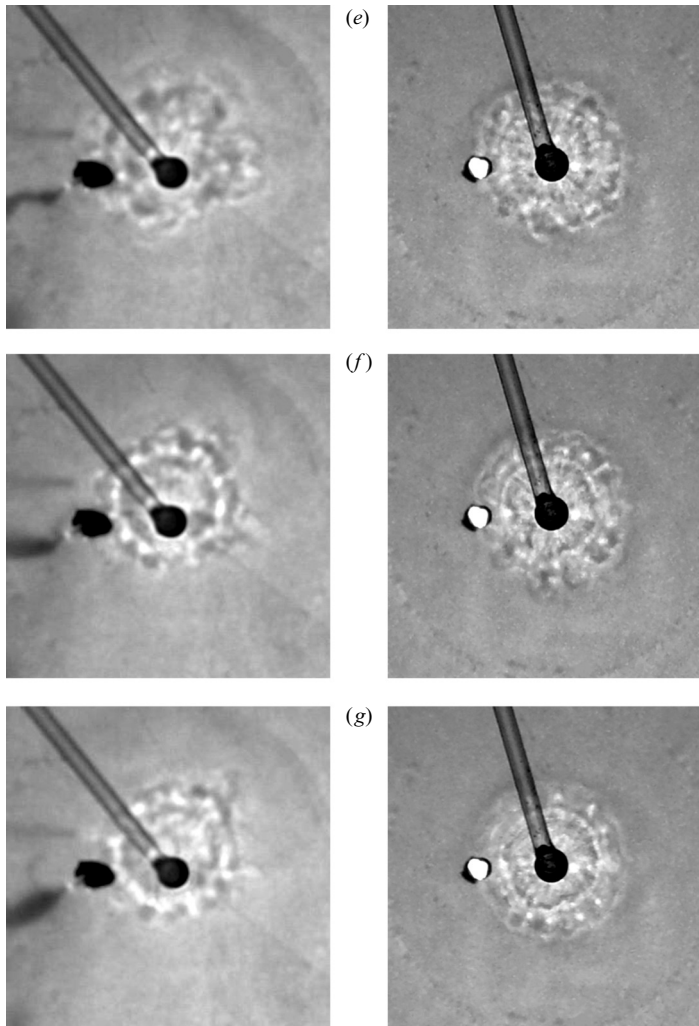


FIGURE 9. Shadowgraph images in experiments with (left) two layers and (right) continuous stratification both with  $Q = 1.26 \text{ cm}^3 \text{ s}^{-1}$ ,  $Re = 353$  and  $g' = 95.1 \text{ cm s}^{-2}$ , at the same times (a) 40 s, (b) 50 s, (c) 60 s, (d) 70 s, (e) 80 s, (f) 90 s, and (g) 100 s, after filling commenced in the 9.35 cm radius pie dish. The photographs are  $7 \text{ cm} \times 7 \text{ cm}$ . Lines from upper left to the centre are the two sides of the filling tube leading to the nozzle. The offset of the nozzle in the two-layer experiment is a result of the non-alignment of the light beam producing the shadowgraph image. The black (left) or white (right) mark to the left of the nozzle is a hole used for injecting a thin wire to which crystals of potassium permanganate are attached to visualize the flow.

pie dish, already submerged in fresh water in the larger tank. The layer was left to settle and diffuse for a period,  $t = 3.17 \text{ h}$ , so forming a continuously stratified layer beneath the fresh water. The thickness of the interface between the upper fresh water layer and the saline layer after this time,  $t$ , is about  $(\pi \kappa_S t)^{1/2}$ , where  $\kappa_S$  is the molecular diffusion coefficient of salt, about  $1.4 \times 10^{-5} \text{ cm}^2 \text{ s}^{-1}$ . The interface thickness is therefore about 7.1 mm after 3.17 h, so producing a stratified layer reaching to the bottom of the tank. A steady flow of saline water of the same density as before was then commenced as in the experiments described in § 2 and with  $Re = 353$ , to produce

a continuously stratified radial shear flow instead of the previous radial two-layer flow. Shadowgraph was used as before to seek evidence of the formation of a circular hydraulic jump.

Figure 9 is a comparison of shadowgraphs obtained in an earlier two-layer experiment (at the left) and one of the present ‘stratified’ experiments (at the right) at the same values of  $Q$  ( $=1.258\text{ cm}^3\text{ s}^{-1}$ ), the same density of the saline fluid ( $g' = 95.1\text{ cm s}^{-2}$ ) and at the same times after the start of filling. In none of the stratified experiments are stable laminar patterns of waves observed, and the diverging flow becomes turbulent close to the injection point. Unlike the formation of waves and the subsequent transition to irregular turbulent motion observed in the two-layer experiments, in the stratified experiments there is relatively little change with time in the appearance of the shadowgraph pattern surrounding the nozzle. At the stage reached at (f) after the waves have disintegrated in the two-layer experiments and the diverging flow has become turbulent close to the nozzle, the patterns in the two-layer experiments are virtually identical to those of the ‘stratified’ experiments.

It is likely that with the removal of the large stabilizing density gradients of the earlier two-layer experiments, the turbulence occurring in the diverging flow close to its point of impact with the horizontal plane in the stratified experiments is a result of shear-induced Kelvin–Helmholtz instability. At times following the onset of mixing in the two-layer experiments, the production of fluid of intermediate density and its intrusion along the interface towards the injection point may result in conditions there that are similar to those in the stratified experiments. This accounts for the similarity of the pattern at the stages shown in figure 9 (f, g). Such changes in density cannot occur in the case of the single-layer circular hydraulic jump.

In the ‘stratified’ experiments, there does, however, appear to be a stationary transition or perhaps a rotor, albeit of a turbulent nature, at a radius similar to that in the later stages of the earlier two-layer flow, suggesting that stationary transitions may still occur in continuously stratified shear flows. Just as in Craik *et al.*'s (1981) experiment, when stationary capillary waves cannot provide a means to transport energy downstream from a jump and, instead of an undular jump, a jump forms with a rotor and an abrupt finite change in level, so too in the stratified case (where stationary waves are precluded but upstream-going waves may occur as explained in §1.3) an abrupt and turbulent jump is found to form.

A possibly important control on upstream wave propagation results from the change in the speed of the mean radial flow approaching the jump. An increase in flow speed as radius decreases, e.g. as in (5), may prevent the upstream propagation of internal waves from a jump. The effects of the divergent flow and viscosity are not insignificant in the present experiments.

In view of their importance in geophysical flows of much greater scale, the conditions in which well-defined jumps or stationary waves can occur in stratified shear flows deserve further investigation.

The first experiments on the circular internal jumps were made in 1983 at the Institute of Oceanographic Sciences with Paul Hutt, and even after a long space of years S.A.T. is most grateful for his help. Further experiments were made by I.K., and much of this was written or developed, at the 2007 GFD Summer School at Woods Hole Oceanographic Institution. Experiments made by I.K. during the Summer School are described in the 2007 Proceedings. We are grateful for Keith Bradley's help and to the organisers for inviting us to attend. I.K.'s work was partly

supported by the Croatian Ministry of Science, Education and Sports under the project “Numerical methods in geophysical models” (No. 037-1193086-2771).

### Appendix A. Waves in two layers with uniform flow or shear in the lower layer

We take  $u = U + \alpha z$  to represent shear in the lower layer of uniform density  $\rho_2$  and thickness  $h$ , and assume the deep upper layer is at rest and of density  $\rho_1$ . Assuming potential flow in the upper layer and that the streamfunction in the lower layer (supposed inviscid) satisfies Rayleigh’s equation (Drazin & Reid 1981, section 23), then on matching the vertical velocity and pressure at a disturbed interface,  $z = h + \eta$ , the equation for the phase speed,  $C$ , of small-amplitude interfacial waves in terms of their wavenumber,  $k$ , is

$$(C - U - \alpha h)^2 + (C - U - \alpha h)(C\rho_1/\rho_2 + \alpha h/kh)\tanh kh = (g'/k)\tanh kh, \quad (\text{A } 1)$$

where  $g' = g(\rho_2 - \rho_1)/\rho_2$ . If  $U = \alpha h = 0$ , (A 1) reduces to the equation for interfacial internal gravity waves:

$$C^2[1 + (\rho_1/\rho_2)\tanh kh] = (g'/k)\tanh kh \quad (\text{A } 2)$$

(Lamb 1932, para 231).

#### A.1. Uniform flow in the lower layer

If  $\alpha h = 0$ , (A 1) reduces to

$$(C - U)^2 + (C - U)(C\rho_1/\rho_2)\tanh kh = (g'/k)\tanh kh. \quad (\text{A } 3)$$

For stationary waves of wavenumber  $k$  with zero wave speed, the flow speed,  $U$ , is given by

$$U^2 = (g'/k)\tanh kh; \quad (\text{A } 4)$$

this is the speed of the waves (stationary in space) measured relative to  $U$ . (For long waves, (A 4) gives  $U^2 = g'h$ , exactly equal to the speed of long-wave propagation if the fluid is at rest with no shear at the interface, i.e. (A 2) with  $U = 0$ . For waves of finite  $kh$ , however, (A 4) gives a speed different from the wave speed (A 2).)

Equation (A4) may be written as

$$Fr \equiv U^2/g'h = \tanh kh/kh, \quad (\text{A } 5)$$

and which must be less than unity; stationary waves can occur only if  $Fr < 1$ . In the limit as  $kh$  tends to zero, (A 3) gives

$$(C - U)^2 = g'h, \quad (\text{A } 6)$$

giving the speed of long waves as  $C = U[1 \pm (1/Fr)^{1/2}]$ . If  $U > 0$ , waves can travel with negative velocity and so contrary to the flow  $U$  only if  $Fr < 1$ .

#### A.2. Uniform shear in the lower layer

Suppose however that there is a shear in the lower layer. Putting  $U = 0$  in (A 1), so that the velocity,  $u = \alpha z$ , satisfies the no-slip boundary condition at  $z = 0$ , we have

$$(C - \alpha h)^2 + (C - \alpha h)(C\rho_1/\rho_2 + \alpha h/kh)\tanh kh = (g'/k)\tanh kh. \quad (\text{A } 7)$$

In the long-wave limit as  $kh$  tends to zero, this gives

$$C^2 - \alpha h C - g'h = 0. \quad (\text{A } 8)$$

The mean speed of the lower layer is  $\langle u \rangle = \alpha h/2$ , and if we write  $Fr = \langle u \rangle^2/g'h$ , (A 8) becomes

$$C^2 - 2\langle u \rangle C - \langle u \rangle^2/Fr = 0. \quad (\text{A } 9)$$

This gives  $C = \langle u \rangle [1 \pm (1 + 1/Fr)^{1/2}]$ , so  $C < 0$  or  $C > \langle u \rangle = \alpha h$ , the maximum flow speed. Unlike the case described above with a uniform flow in the lower layer, the speed of long waves lies outside the range (0 to  $\alpha h$ ) of  $u$ .

Differentiating (A 7) with respect to  $k$ , we find an equation for the group velocity,  $C_g = \partial\sigma/\partial k$ . In the limit as  $kh$  tends to zero,  $C_g = C$ , and long-wave energy travels at the speed of propagation of the long waves.

A remarkable feature is that long waves can therefore propagate energy upstream whatever the value of  $Fr$ .

Waves can however remain stationary in the flow. Using (A7), the condition for stationary waves,  $C = 0$ , becomes

$$4\langle u \rangle^2 = (g'h)\tanh kh/(kh - \tanh kh). \quad (\text{A } 10)$$

The corresponding Froude number,  $Fr \equiv \langle u \rangle^2/(g'h)$  is equal to  $\tanh kh/[4(kh - \tanh kh)]$ . This is continuous as  $kh$  increases, and tends to  $3/(4k^2h^2)$  as  $kh$  tends to zero and to zero as  $kh$  tends to infinity: stationary waves can be found for all values of  $Fr$ .

With  $Q = 2\pi rh\langle u \rangle$ , (A 10) gives

$$x^3 \tanh x/[4(x - \tanh x)] = \Phi, \quad (\text{A } 11)$$

where  $\Phi = 2\pi Q^2/r^2 g'\lambda^3$  as in (3) and  $x = kh = 2\pi h/\lambda$ , so that, as in §3.1,  $h$  can be determined if the terms on the right-hand side of (A 11) are known. Equation (A 11) leads to greater (or smaller) values of  $h$  than (3) if  $\Phi >$  (or  $<$ ) 0.827. If  $\Phi = 0.5$ , ((3): no shear) gives values of  $h$  that are 31 % greater than ((A 11); with shear), and if  $\Phi = 1.5$ , (3) gives values of  $h$  that are 30 % less than (A 11).

## Appendix B. Flow beyond the jump

Suppose that there is a steady potential inviscid flow in the lower layer of density  $\rho_2$  at radii beyond that of the jump,  $r_1$ . A solution for the velocity potential,  $\phi$ , that satisfies  $\nabla^2\phi = 0$ , is

$$\phi = U_1 r_1 (z^2 - r^2/2 + R^2 \log r)/(R^2 - r_1^2). \quad (\text{B } 1)$$

This satisfies the boundary conditions

$$u = \partial\phi/\partial r = U_1 \text{ at } r = r_1, \quad 0 \leq z \leq h'_2, \quad (\text{B } 2)$$

where  $h'_2$  is the value of  $h_2$  just downstream of the jump at  $r = r_1$ , and

$$u = \partial\phi/\partial r = 0 \text{ at an outer boundary, } r = R, \quad (\text{B } 3)$$

assuming the boundary is circular and vertical, in addition to

$$w = \partial\phi/\partial z = 0 \text{ at } z = 0. \quad (\text{B } 4)$$

The velocity components are  $u = U_1 r_1 (R^2 - r^2)/[r(R^2 - r_1^2)]$ , and  $w = 2U_1 r_1 z/(R^2 - r_1^2)$ . The radial velocity,  $u$ , differs from the inviscid solutions of Watson (1994) for flow spreading radially from the nozzle into a region unlimited in horizontal dimension.

We suppose that the depth,  $h_2$ , of the lower layer is much less than the radius of the container,  $R$ , and it follows that  $u \gg w$  except within a distance of a few times



the depth from the outer boundary. Supposing the pressure at  $r = r_1$ ,  $z = h'_2$ , is  $p_0$ , applying Bernoulli's theorem in the lower layer, neglecting  $w$  in comparison with  $u$ , time variations in  $U_1$  (valid if  $dU_1/dt \ll U_1^2/L$  where  $L$  is the tank width) and equating the pressure at  $z = h_2$  to that in the stationary and hydrostatic overlying layer,  $p_0 - g\rho_1(h - h_2)$ , after some algebraic manipulation we obtain

$$h_2 = h'_2 + (U_1^2 r_1^2)(R^4 - r_1^2 r_1^2)(r^2 - r_1^2)/[2g'r^2 r_1^2(R^2 - r_1^2)^2]. \quad (\text{B } 5)$$

If  $Fr'_2 = U_1^2/g'h'_2$  is a Froude number based on the layer depth  $h'_2$  we find

$$\langle h_2 \rangle = \int_{r_1}^R h_2 2\pi r \, dr / [\pi(R^2 - r_1^2)] = h'_2(1 + Fr'_2 \Theta) \quad (\text{B } 6)$$

where, if  $x_0 = r_1/R$ ,

$$\Theta = (2 - x_0^2 + x_0^4)[4(1 - x_0^2)^2] + x_0^2 \log x_0 / (1 - x_0^2)^3. \quad (\text{B } 7)$$

For small values of  $x_0$ , as in the experiments,  $\Theta \approx \frac{1}{2}$  and  $\langle h_2 \rangle \approx h'_2(1 + Fr_2/2)$ . This is less than  $3h'_2/2$ , if  $Fr'_2 < 1$ .

The mean value,  $\langle h_2 \rangle$ , of the layer depth beyond the jump estimated from the inflow,  $Q$ , and time may exceed the layer depth just downstream of the jump,  $h'_2$ , by a factor of up to 50%, leading to estimates of  $Fr_2 = Q^2/(4\pi^2 r_1^2 g' \langle h_2 \rangle^3)$  that are as much as one-third of  $Fr'_2$ . In practice the estimate gives, at best, an approximate guide to the value of  $\langle h_2 \rangle$  because the tank is not circular and the flow is not inviscid, but this provides a rough measure of the substantial uncertainty involved in the use of  $\langle h_2 \rangle$  as the depth of the layer,  $h'_2$ , at the jump.

## Appendix C. The spreading layer and the location of the jump

### C.1. The viscosity-affected flow in the lower layer

Following Watson (1964) we suppose the lower layer is of density  $\rho_2$  and of thickness  $h(r)$  at radius  $r$  from the nozzle. At small values of  $r$ , the flow,  $U_0$ , from the nozzle (of radius  $a$ ) is undiminished, and

$$Q = \pi a^2 U_0 = 2\pi r h U_0, \quad (\text{C } 1)$$

where  $Q$  is the flow rate, and so

$$r h = a^2/2. \quad (\text{C } 2)$$

We assume that the effects of viscosity and loss of momentum within the lower layer resulting from the stress on the horizontal plane and at the interface between the two layers spread vertically from the lower boundary and the interface into the lower layer, eventually modifying the flow throughout the layer at some radius  $r_0$ , as sketched in figure 6. At greater radii the flow speed in the layer is assumed to be given in a self-similar form,  $u(r, z) = U(r)f(\eta)$ , where  $U$  is the maximum flow speed and  $f$  is a function of  $\eta = z/h$ . Since the upper layer exerts a stress at the interface that acts to retard the lower layer (or equivalently motion in the upper layer is driven by the viscous drag of the moving lower layer) then  $f' = df/d\eta < 0$  at  $z = h$  (i.e.  $f'(1) < 0$ ). The maximum flow,  $U$ , is found in the lower layer at a level  $\eta = \eta_* < 1$  where  $f' = 0$ . Furthermore  $0 \leq f(1) \leq 1$ ; the lower bound (zero) is found when the upper layer is immobile, e.g. when its viscosity is relatively very large, and the upper bound (unity) is when the upper layer is inviscid (and the solution becomes that considered by Watson with zero stress at the upper boundary). In practice, the upper layer will have

properties between these limits and we expect that  $f(1)$  exceeds zero but is less than unity.

Following Watson, by continuity the volume flux in the lower layer is

$$Q = 2\pi r \int_0^{h(r)} u \, dz = 2\pi r U h \int_0^1 f(\eta) \, d\eta, \quad (\text{C } 3)$$

and

$$rUh = c_1 Q, \quad (\text{C } 4)$$

where  $c_1$  is a dimensionless constant, independent of  $r$ , and equal to  $1/[2\pi \int_0^1 f(\eta) \, d\eta]$ . The vertical velocity,  $w = Uh' \eta f(\eta)$ , is derived from  $\text{div } \mathbf{u} = 0$ . Neglecting the horizontal pressure variation in the lower layer, the equation of conservation of horizontal momentum gives  $h^2 U' f^2 = \nu f''$ , where  $\nu$  is the viscosity of the lower layer. This implies that for constant kinematic viscosity,  $\nu$ , the product  $h^2 U'$  is a constant which we choose as  $-3c^2 \nu/2$ , where  $c$  is a non-dimensional constant, taken to be positive. (The derivative of  $f$  decreases through the layer and so  $f'' < 0$ .) It follows that

$$f'' = -3c^2 f^2/2. \quad (\text{C } 5)$$

Integrating we find

$$f' = c(1 - f^3)^{1/2} \quad \text{if } 0 \leq \eta \leq \eta_*, \quad (\text{C } 6a)$$

so  $f' = c$  when  $\eta = 0$  since  $f(0) = 0$ , and

$$f' = -c(1 - f^3)^{1/2} \quad \text{if } \eta_* \leq \eta \leq 1. \quad (\text{C } 6b)$$

Integrating (C 6a) from  $\eta = 0 (f = 0)$  to  $\eta_* (f = 1)$  we find

$$c\eta_* = \int_0^1 (1 - f^3)^{-1/2} \, df \approx 1.402 \quad (\text{C } 7a)$$

(Watson's equation (20)), whilst integration of (C 6b) gives

$$c(1 - \eta_*) = \int_{f(1)}^1 (1 - f^3)^{-1/2} \, df. \quad (\text{C } 7b)$$

Adding these equations we obtain

$$c \approx 2.804 - \int_0^{f(1)} (1 - f^3)^{-1/2} \, df. \quad (\text{C } 8)$$

Noting that, for example, (C 6a) may be written as  $(1 - f^3)^{-1/2} \, df = c \, d\eta$ , multiplying by  $f$  and integrating (C 6a) and (C 6b) we find

$$\begin{aligned} \int_0^1 f \, d\eta &= c^{-1} \left[ \int_0^1 f(1 - f^3)^{-1/2} \, df + \int_{f(1)}^1 f(1 - f^3)^{-1/2} \, df \right], \\ &\approx c^{-1} \left[ 1.725 - \int_0^{f(1)} f(1 - f^3)^{-1/2} \, df \right], \end{aligned}$$

since (as shown by Watson),  $\int_0^1 f(1 - f^3)^{-1/2} df \approx 0.8625$ . Hence

$$c_1 \approx c \left[ 1.725 - \int_0^{f(1)} f(1 - f^3)^{-1/2} df \right]^{-1}. \quad (\text{C } 9)$$

From (C 4) and the equation  $h^2 U' = -3c^2 v/2$ , we find

$$U(r) = 2c_1^2 Q^2 / [c^2 v(r^3 + l^3)] \quad (\text{C } 10)$$

and

$$h(r) = c^2 v(r^3 + l^3) / [2Qc_1 r] \quad (\text{C } 11)$$

where  $l$  is a constant length.

Like Watson, we assume that a boundary layer grows upwards from the plane  $z = 0$  into the layer flowing at speed  $U_0$  but also that a second layer grows downwards into the lower layer from its upper boundary. The total extent of these layers at radius  $r$  is proportional to  $(\nu t)^{1/2}$  where  $t$  is the time,  $r/U_0$ . The boundary layers will extend across the moving lower layer when  $(\nu r/U_0)^{1/2}$  is of order  $h$ , that is (using (C 1) and (C 2)) at a radius,  $r_0$ , proportional to  $aRe^{1/3}$ , where  $Re = U_0 a/\nu = Q/\pi v a$  is the Reynolds number of the flow in the nozzle. At  $r = r_0 -$  (the limit as  $r_0$  is approached from below), however, the maximum flow still (just) unaffected by the boundary layers is  $U_0$ , and matching to the similarity solution (C 10) at  $r = r_0 +$ , we find

$$U_0 = 2c_1^2 Q^2 / [c^2 v(r_0^3 + l^3)], \quad (\text{C } 12)$$

which leads to

$$l^3 = 2c_1^2 Q^2 / c^2 v U_0 - r_0^3 = 2\pi c_1^2 a^3 Re / c^2 - r_0^3, \quad (\text{C } 13)$$

and so  $l$  is also proportional to  $aRe^{1/3}$ .

### C.2. The location of the jump

Suppose that a hydraulic jump occurs at radius  $r_1 > r_0$ , where the similarity solution is expected to hold. Supposing that the radial extent of the jump is small (a limitation discussed in Appendix D) and that there is a layer of uniform velocity  $U_1$  and thickness  $h_2$  downstream of the jump, conservation of momentum (the net downstream pressure force leading to a change in momentum flux), gives

$$\rho_2 g' (h_1^2 - h_2^2) / 2 = \rho_2 U_1^2 h_2 - \rho_2 \int_0^h u^2 dz + \rho_2 m, \quad (\text{C } 14)$$

at  $r = r_1$ . Here  $g' = g(\rho_2 - \rho_1) / \rho_2$ , accounting for a hydrostatic pressure exerted by the upper layer of density  $\rho_1$  on the lower layer. We include the term  $\rho_2 g' h_1^2 / 2$  representing the pressure in the lower layer upstream of the jump, a term omitted by Watson consistent with his assumption that  $h_1^2 / h_2^2 \ll 1$ . The term  $\rho_2 m$  represents the flux of momentum that is radiated downstream by internal waves or lost in the transition by viscous stress at the boundaries of the layer. Using the equation of continuity of flux,  $Q$ , in the layer downstream of the transition (C 14) gives

$$r_1 (h_2^2 - h_1^2) g' a^2 / Q^2 + a^2 / (2\pi^2 r_1 h_2) + M = (2r_1 a^2 / Q^2) \int_0^h u(r_1, z)^2 dz, \quad (\text{C } 15)$$

where

$$M = 2r_1 a^2 m / Q^2. \quad (\text{C } 16)$$

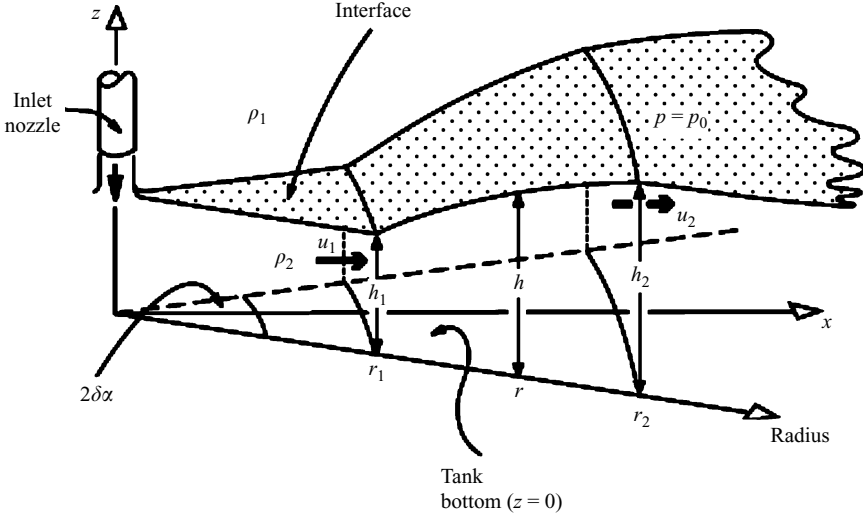


FIGURE 10. Notation for a two-layer transition of finite radial width,  $r_2 - r_1$ , within a radial segment of angle  $2\delta\alpha$ . The height of the stippled interface above the bottom of the tank at level  $z=0$  increases from  $h_1$  at  $r=r_1$  to  $h_2$  at  $r=r_2$ , and the radial flow changes from  $u_1$  to  $u_2$ .

When  $r > r_0$ , the velocity  $u = Uf$ , and  $U$  and  $h$  are given by (C 10) and (C 11), so at  $r = r_1$ :

$$\int_0^h u(r_1, z)^2 dz = U^2 h \int_0^1 f^2 d\eta = \{2c_1^3 Q^3 / [c^2 \nu r_1 (r_1^3 + l^3)]\} \int_0^1 f^2 d\eta. \quad (\text{C } 17)$$

Using the equation of continuity of flux across the transition and the definition of  $c_1$ , we can write

$$r_1 h_1^2 g' a^2 / Q^2 = \{g' a^4 c^4 [(r_1/a)^3 + (l/a)^3]^2\} / 4\pi^4 r_1 \nu^2 c_1^2 Re^4. \quad (\text{C } 18)$$

Substituting these expressions, using  $Re = Q/\pi a \nu$ , and evaluating  $\int_0^1 f^2 d\eta$  using (C 5), (C 15) leads to the equation

$$Y = Z, \quad (\text{C } 19)$$

where

$$Y = r_1 h_2^2 g' / (\pi \nu Re)^2 + a^2 / (2\pi^2 r_1 h_2) + M,$$

and

$$\begin{aligned} Z = & \{8\pi c_1^3 Re / (3c^3 [(r_1/a)^3 + (l/a)^3])\} [1 - f'(1)/c] \\ & + g' a^4 c^4 [(r_1/a)^3 + (l/a)^3]^2 / (4\pi^4 r_1 \nu^2 c_1^2 Re^4), \end{aligned}$$

provided  $r_1 > r_0$ .

#### Appendix D. Conservation laws in jumps of finite width in inviscid radial flows

Consider the outward radial flow in a layer of density  $\rho_2$  through a transition that lies within a segment of angle  $2\delta\alpha$  from  $r_1$  to  $r_2$  about a direction,  $x$ , as shown in figure 10, where the layer depth at  $r_1$  is  $h_1$  and at  $r_2$  is  $h_2$ . The overlying layer is at rest

and of density  $\rho_1$ . If the pressure,  $p$ , is hydrostatic and equal to  $p_0$  at a height  $h_2$ , then to order  $\delta\alpha$ , the outward pressure force in direction  $x$  at radius  $r_1$  is  $2\delta\alpha r_1 \int p dz$  from  $z=0$  to  $z=h_2$ , which is equal to  $2\delta\alpha r_1 [p_0 h_2 + g\rho_1(h_2 - h_1)^2 + g\rho_2 h_1^2]$ . The corresponding inward force at radius  $r_2$  is  $2\delta\alpha r_2 \int p dz$  from  $z=0$  to  $z=h_2$ , which is equal to  $2\delta\alpha r_2 [p_0 h_2 + g\rho_2 h_2^2]$ . An  $x$ -directed outward pressure force on the sides of the segment equal to twice the double integral of the pressure from  $z=0$  to  $z=h_2$ , and from  $r_1$  to  $r_2$ , times  $\sin \delta\alpha$ , gives a further force  $2\delta\alpha [p_0 h_2 (r_2 - r_1) + g\rho_1 h_2^2 (r_2 - r_1)/2 + g(\rho_2 - \rho_1) \int h^2 dr]$  if  $\delta\alpha \ll 1$ , where the integral is from  $r_1$  to  $r_2$  and where  $h(r)$  is the height of the interface between  $r_1$  and  $r_2$ . Summing these terms, the net outward force acting on fluid in the segment is  $2\delta\alpha g(\rho_2 - \rho_1) [(r_1 h_1^2 - r_2 h_2^2)/2 + \int h^2 dr]$ .

(The last of these force terms is absent in parallel channel flows. If the pressure forces on the sides of the segment shown in figure 10 are ignored, the pressure,  $p_0$ , at  $z=h_2$  leads to an  $x$ -directed pressure force,  $2\delta\alpha r_1 p_0 h_2$  at the inner radius,  $r_1$ , that is not balanced by the corresponding force,  $2\delta\alpha r_2 p_0 h_2$  at the outer radius,  $r_2$ , and leaves a term containing  $p_0$  in the expression for  $Fr_1$ . This effect of a finite width transition appears to have been overlooked in the transition in a single layer where  $p_0$  is taken to be zero. In the expression for the work done by the pressure the related terms are  $2\delta\alpha r_1 p_0 h_1 u_1$  at  $r_1$  and  $2\delta\alpha r_2 p_0 h_2 u_2$  at  $r_2$ , and these are equal because of the continuity of volume flux. There is no normal component of velocity through the sides of the sector and the work done there by the pressure is zero.)

If we neglect the entrainment of fluid from the upper layer into the lower, this net outward force leads to a rate of change in the  $x$ -directed momentum of fluid passing through the segment, equal to  $2\delta\alpha [\rho_2 r_2 h_2 u_2^2 - \rho_2 r_1 h_1 u_1^2]$ , correct only to order  $\delta\alpha$  because of the spreading field of motion, where  $u_i$  is the velocity supposed uniform over the vertical sector normal to the flow at radius  $r_i$ ,  $i=1, 2$ . Equating the net force and the rate of change of momentum in direction  $x$  (and, in the inviscid flow, neglecting momentum loss through the stress on the lower boundary) gives

$$\rho_2 (r_2 h_2 u_2^2 - r_1 h_1 u_1^2) = g(\rho_2 - \rho_1) \left[ (r_1 h_1^2 - r_2 h_2^2) + \iint h^2 dr \right] / 2. \quad (D 1)$$

Writing  $R = r_2/r_1$  (a jump width parameter),  $q = h_2/h_1$  (the jump amplitude),  $y = h/h_1$ , and  $x = r/r_1$ , and using the continuity equation,  $Q = 2\pi r_1 u_1 h_1 = 2\pi r_2 u_2 h_2$ , (D 1) reduces to

$$Fr_1 \equiv u_1^2/g'h_1 = qR \left[ Rq^2 - 1 - \int_1^R y^2 dx \right] / [2(qR - 1)], \quad (D 2)$$

an equation for the Froude number,  $Fr_1$ , at the transition in terms of possibly measurable, but as yet unavailable, quantities, e.g.  $q$ ,  $R$  and  $y$ , defining the transition's shape. If  $R = 1$ , an abrupt jump, we recover the equation  $Fr_1 = q(q + 1)/2$ , familiar in channel flows, but in a radial flow of one or two layers additional terms are present in jumps of finite width when  $R \neq 1$ .

The rate of loss of the radial flux of energy,  $2\pi r [\int (\rho u)^2/2) u dz + \int p u dz + \int (g\rho z) u dz]$ , presents no problem similar to that of the (directional) momentum, and is found to be

$$E_{loss} = 2\pi [\rho_1 u_1^3 h_1 r_1/2 - \rho_2 u_2^3 h_2 r_2/2 - u_1 h_1 r_1 g(\rho_2 - \rho_1)(h_2 - h_1)], \quad (D 3)$$

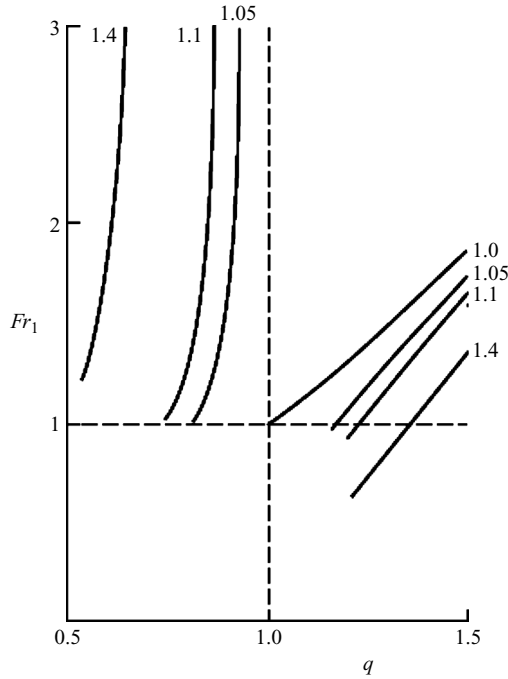


FIGURE 11. The relation between wave amplitude,  $q$ , and internal Froude number,  $Fr_1$ . Curves are labelled with values of the jump width parameter,  $R$ .

after use of the continuity equation. Substituting for  $q$  and  $R$  and putting  $\rho_2 \approx \rho_1$ , leads to

$$E_{loss} = \pi \rho_2 u_1 h_1^2 r_1 g' \{ (u_1^2 / g' h_1) [1 - 1 / (Rq)^2] - 2(q - 1) \}, \quad (\text{D } 4)$$

which, with no supply of energy in the transition from  $r_1$  to  $r_2$ , must be  $\geq 0$ . We therefore require that

$$Fr_1 [1 - 1 / (Rq)^2] - 2(q - 1) \geq 0, \quad (\text{D } 5)$$

with  $Fr_1 = u_1^2 / g' h_1$ , given by (D 2).

If  $R = 1$  (i.e. an abrupt change in level or a very thin transition) (D 4) gives

$$E_{loss} / 2\pi = [\rho_2 u_1 h_1 r_1 g' / 4q] (q - 1)^3, \quad (\text{D } 6)$$

so, for a loss in energy flux,  $q \geq 1$ . This is the familiar result in single- or two-layer channel flows. For a non-negative loss in energy flux, from (D 6),  $q$  must be greater than 1 and, from  $Fr_1 = q(q + 1) / 2$ , it follows that  $Fr_1 \geq 1$ .

A radial flow with a transition of finite width does not always have a critical value,  $Fr_1 = 1$ . If, for example,  $h$  is continuous with a quadratic shape and with  $dh/dr = 0$  at  $h = h_2$ , corresponding approximately to the height profiles measured by Craik *et al.* (1981); their figure 6), then  $\int_1^R y^2 dx = (R - 1)[1 + 4(q - 1) / 3 + 8(q - 1)^2 / 15]$ . For  $R > 1$ , values of  $Fr_1 > 0$  given by (D 2) that satisfy the condition (D 5) lie on the pairs of curves shown in figure 11. One set of curves (those on the right of the figure) have  $q > 1$  but with values of  $Fr_1$  that may be less than unity for the smaller values of  $q$ , whilst the other has  $q < 1$  and  $Fr_1 > 1$ .

It appears that finite width transitions can occur at values of  $Fr_1$  that are less than unity, or at values of  $q < 1$  (a reduction in the layer thickness), although their stability and related physical existence have not been addressed and remain in doubt.

## REFERENCES

- BAINES, P. G. 1995 *Topographic Effects in Stratified Flows*. Cambridge University Press.
- BELL, T. H. 1974 Effects of shear on the properties of internal gravity waves. *Deutsche Hydrograph Z.* **27**, 57–62.
- BOHR, T., DIMON, P. & PUTKARADZE, V. 1993 Shallow water approach to the circular hydraulic jump. *J. Fluid Mech.* **254**, 635–648.
- BOWLES, R. & SMITH, F. 1992 The standing hydraulic jump: Theory, computations and comparisons with experiments. *J. Fluid Mech.* **242**, 145–168.
- BROWN, G. L. & ROSHKO, A. 1974 On the density effects and large structure in turbulent mixing layers. *J. Fluid Mech.* **64**, 775–816.
- BUSH, J. & ARISTOFF, J. 2003 The influence of surface tension on the circular hydraulic jump. *J. Fluid Mech.* **489**, 229–238.
- BUSH, J. W. M., ARISTOFF, J. M. & HOSOI, A. E. 2006 An experimental investigation of the stability of the circular hydraulic jump. *J. Fluid Mech.* **558**, 33–52.
- CRAIK, A., LATHAM, R., FAWKES, M. & GIBBON, P. 1981 The circular hydraulic jump. *J. Fluid Mech.* **112**, 347–362.
- DRAZIN, P. G. & REID, W. H. 1981 *Hydrodynamic Stability*. Cambridge University Press, Cambridge.
- DUNCAN, J. H., QIAO, H., PHILOMIN, V. & WENZ, A. 1999 Gentle spilling breakers: crest profile evolution. *J. Fluid Mech.*, **379**, 191–222.
- HASSID, S., REGEV, A. & POREH, M. 2007 Turbulent energy dissipation in density jumps. *J. Fluid Mech.* **572**, 1–12.
- HIGUERA, F. 1994 The hydraulic jump in a viscous laminar flow. *J. Fluid Mech.* **274**, 69–92.
- HOLLAND, D. M., ROSALES, R. R., STEFANICA, D. & TABAK, E. G. 2002 Internal hydraulic jumps and mixing in two-layer flows. *J. Fluid Mech.* **470**, 63–83.
- LAMB, H. 1932 *Hydrodynamics*, 6th edn. Cambridge University Press.
- LIGHTHILL, J. 1978 *Waves in Fluids*. Cambridge University Press.
- LONGUET-HIGGINS, M. S. 1992 Capillary rollers and bores. *J. Fluid Mech.* **240**, 659–679.
- POLZIN, K., SPEER, K. G., TOOLE, J. M. & SCHMITT, R. W. 1996 Intense mixing of Antarctic Bottom Water in the equatorial Atlantic Ocean. *Nature* **380**, 54–56.
- RAYLEIGH, LORD 1914 On the theory of long waves and bores. *Proc. R. Soc. Lond. A* **90**, 324–327.
- SCORER, R. 1972 *Clouds of the World*. Melbourne, Lothian Pub. Co.
- SIMPSON, J. E. 1997 *Gravity Currents in the Environment and the Laboratory*, 2nd edn. Cambridge University Press.
- THORPE, S. A. 2007 Dissipation in hydraulic transitions in flows through abyssal channels. *J. Mar. Res.* **65**, 147–168.
- THORPE, S. A. & OZEN, B. 2007 Are cascading flows stable? *J. Fluid Mech.* **589**, 411–432.
- THURNHERR, A. M., ST LAURENT, L. C., SPEER, K. G., TOOLE, J. M. & LEDWELL, J. R. 2005 Mixing associated with sills in a canyon on the mid-ocean ridge flank. *J. Phys. Oceanogr.* **35**, 1370–1381.
- TURNER, J. S. 1973 *Buoyancy Effects in Fluids*. Cambridge University Press.
- WATSON, E. M. 1964 The spread of a liquid jet over a horizontal plane. *J. Fluid Mech.* **20**, 481–499.
- WILKINSON, D. L. & WOOD, I. R. 1971 A rapidly varied flow phenomenon in a two-layer flow. *J. Fluid Mech.* **47**, 241–256.